# Graphene Photonics, Plasmonics, and Broadband Optoelectronic Devices

**Qiaoliang Bao[†,‡] and Kian Ping Loh[†,‡,*]**

[†]Graphene Research Centre, National University of Singapore, 6 Science Drive 2, Singapore 117546, and [‡]Department of Chemistry, National University of Singapore, 3 Science Drive 3, Singapore 117543

**ABSTRACT** Graphene has been hailed as a wonderful material in electronics, and recently, it is the rising star in photonics, as well. The wonderful optical properties of graphene afford multiple functions of signal emitting, transmitting, modulating, and detection to be realized in one material. In this paper, the latest progress in graphene photonics, plasmonics, and broadband optoelectronic devices is reviewed. Particular emphasis is placed on the ability to integrate graphene photonics onto the silicon platform to afford broadband operation in light routing and amplification, which involves components like polarizer, modulator, and photodetector. Other functions like saturable absorber and optical limiter are also reviewed.

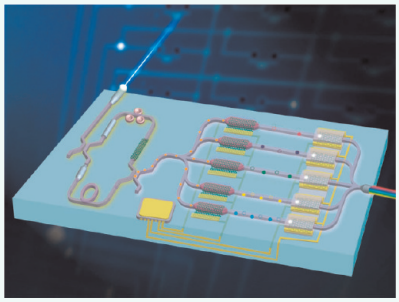

**KEYWORDS:** graphene · photonics · optoelectronics · broad band · ultrafast laser · saturable absorber · polarizer · optical modulator · photodetector · optical limiter

Silicon photonics has been hailed as the technology of promise which will make super-high-speed Internet access a reality. In reality, progress toward a photonics-driven circuit is hampered by problems in the downscaling and integration of optoelectronic hardware. The present state of development in integrated photonics is not unlike the integrated circuit revolution more than 50 years ago. Breakthroughs similar to what silicon transistors had achieved for integrated circuits are critically needed for integrated photonics before it can take off in a big way.

It is good to remind ourselves why silicon, which is prevalent in electronics, is also a favorite choice in photonics. The main reason is its amenability to the monolithic integration of optics and electronics.[1] Silicon-based photonic components ranging from passive devices to modulators, detectors, and light amplifiers and sources have been developed.[1−3] However, it is unlikely that all of the photonic components can be silicon-based, especially when there is a need to fulfill the stringent demands of broadband data transferring. First of all, intrinsic silicon, which has an indirect band gap, is not a broadband optical material even though its absorption edge can be tuned by controlling the doping level.[4] Other drawbacks inherent to silicon include low electro-optic coefficient, low light emission efficiency, and high propagation losses due to scattering off the side walls of the waveguide. To this end, the fabrication of hybrid materials which can marry the advantages of silicon and a second broadband photonic material seems the most promising way forward.

Graphene, a conjugated $sp^2$ carbon sheet arranged in a two-dimensional (2D) hexagonal lattice,[5,6] is the new kid on the block for electronics[7,8] as well as photonics.[9−11] The wonderful properties of graphene allow multiple functions of signal emitting, transmitting, modulating, and detection to be realized in one material. Graphene shows superior properties compared to silicon and III−V semiconductors in terms of its high thermal conductivity (~36 times higher than Si and ~100 times higher than GaAs), high optical damage threshold[12] (a few orders of magnitude higher than Si[13] and GaAs[14]), and high third-order optical nonlinearities (~$10^{-7}$ esu),[15,16] as shown in Table 1.[17−21] These macroscale properties are important for photonic devices. At present, the Holy Grail for graphene growth is to deposit graphene directly on insulators such as $SiO_2$,[22,23] this is an eagerly awaited breakthrough which will open up a route for monolithic integration of graphene and silicon photonics.[24] The prospect of integrating a graphene photodetector in CMOS (complementary metal−oxide−semiconductor) in the near future is particularly alluring. Recently, an IBM group demonstrated the use of graphene as an optical receiver operating on a silicon-on-insulator (SOI) substrate.[25] A Berkeley photonics group has also successfully integrated graphene with a Si waveguide to fabricate a radio frequency

* Address correspondence to chmlohkp@nus.edu.sg.

Received for review March 6, 2012 and accepted April 18, 2012.

**Published online April 18, 2012**
10.1021/nn300989g

optical modulator.[26] These successes are the first milestones toward hybrid silicon–graphene photonic circuits.

**The Optics Vision.** Due to the unique electronic structure in which conical-shaped conduction and valence bands meet at the Dirac point, the optical conductance of pristine monolayer graphene is frequency-independent in a broad range of photon energies: $G_1(\omega) = G_0 \equiv e^2$, where $\omega$ is the radian frequency, $e$ is electron charge, and $\hbar$ is reduced Planck's constant.[27−30] As a direct consequence of this universal optical conductance, the optical transmittance of pristine graphene is also frequency-independent and solely determined by the fine structure constant $\alpha = e^2/\hbar c$ ($c$ is the speed of light):

$$T \equiv (1+2\pi G/c)^{-2} \approx 1 - \pi\alpha \approx 0.977 \quad (1)$$

When scaled to its atomic thickness, graphene actually shows strong broadband absorption per unit mass of the material ($\pi\alpha$ = 2.3%, Figure 1a), which is ~50 times higher than GaAs of the same thickness.[29,31,32] The reflectance under normal light incidence is relatively weak and written as $R = 0.25\pi^2\alpha^2T = 1.3 \times 10^{-4}$, which is much smaller than the transmittance.[28] The absorption of few-layer graphene can be roughly estimated by scaling the number of layers ($T \cong 1 - N\pi\alpha$). In principle, a low sheet resistance can be attained without sacrificing the properties of transparency too much (*i.e.*, tens of Ω/□ for $T > 90\%$). As such, graphene enthusiasts are hopeful that few-layer graphene can potentially replace ITO (indium tin oxide) as transparent conductors for applications in solar cells[33−35] and touch screens[9,36,37] in cases when it is sufficiently doped.

The property of graphene is largely controlled by the chemical potential ($\mu$, also Fermi level $E_F$). The transition from dielectric to metallic behavior in terms of optical transition[32,38] can be tuned by chemical doping or electrical gating, as schematically illustrated in Figure 1b,c. Within the random-phase approximation, the dynamic optical response of graphene can be derived from Kubo formula in a complex form consisting of interband and intraband contributions[27,30,39]

$$\sigma = \sigma_{intra} + \sigma_{inter}' + i\sigma_{inter}'' \quad (2)$$

where the intraband conductivity $\sigma_{intra}$ has the Drude-like form

$$\sigma_{intra} = \sigma_0 \frac{4\mu}{\pi} \frac{1}{\hbar\tau_1 - i\hbar\omega} \quad (3)$$

where $\sigma_0 = \pi e^2/(2h)$, $\tau_1$ is the relaxation rate associated with intraband transitions, and $\mu > 0$ is the chemical potential. The interband contribution has the form

$$\sigma_{inter}' = \sigma_0\left(1 + \frac{1}{\pi}\arctan\frac{\hbar\omega - 2\mu}{\hbar\tau_2} - \frac{1}{\pi}\arctan\frac{\hbar\omega + 2\mu}{\hbar\tau_2}\right) \quad (4)$$

and

$$\sigma_{inter}'' = -\sigma_0\frac{1}{2\pi}\ln\frac{(2\mu+\hbar\omega)^2 + \hbar^2\tau_2^2}{(2\mu - \hbar\omega)^2 + \hbar^2\tau_2^2} \quad (5)$$

where $\tau_2$ is the relaxation rate associated with interband transitions.

**VOCABULARY: photonics** – the science and applied technology involves the generation, emission, transmission, modulation, signal processing, switching, amplification, detection, and sensing of light · **polarizer** – a device that converts a beam of light with undefined or mixed polarization into a beam with well-defined polarization · **optical modulator** – a device that is used to vary the fundamental characteristics (amplitude, phase, or polarization) of a light beam propagating either in free space or in an optical waveguide upon external electric field · **photodetector** – a device that measures photon flux or optical power by converting the energy of the absorbed photons into a measurable form. It has two principal classes: photoelectric detector and thermal detector · **saturable absorption** – a property of materials where the absorption of light is decreased to a steady level at sufficiently high incident light intensity · **saturable absorber** – an optical material that is used in laser cavities to reshape laser pulses due to saturable absorption. The key parameters for a saturable absorber are its working wavelength, dynamic response, modulation depth, and saturation intensity · **optical limiter** – a kind of nonlinear optical device that strongly attenuates intense optical beams while exhibiting high transmittance for low-intensity ambient light ·

According to above equations, both interband and intraband conductivities are closely correlated with the chemical potential of graphene and the frequency of incident light. The chemical potential of doped graphene is determined by the carrier concentration $n_0 = (\mu/\hbar v)^2/\pi$, which can be controlled *via* chemical doping or electrical gating. There is no intraband contribution for pristine graphene which has $\mu = 0$. Due to the occurrence of zero band gap, the intraband and interband contributions compete and the interband transition only occurs above the threshold of $|\mu| = \hbar\omega/2$, as shown in Figure 1d. Generally, for slightly doped graphene ($|\mu| < \hbar\omega/2$), the high-frequency dynamic conductivity is dominated by interband contribution for Dirac fermions extending across a wide bandwidth from visible to infrared (IR), which covers the telecommunication bands and also the mid-IR regions. The intraband contribution will only be relevant in the terahertz range when $|\mu| > \hbar\omega/2$ (Figure 1d); this condition allows for plasmon momentum enhancement, and thus propagation of surface plasmon in graphene is possible.[40−42] As a result, the relative contributions from optical interband transition and intraband transition can be varied, leading to tunable optical response[32,38] as well as polarization-selective coupling.[26,43]

**Nonlinear Effects in Graphene.** The optical nonlinearities originate from the interactions of the optical field with electrons and phonons. Specifically, the electric field of the optical signal resonates with the electrons in the outer shells of carbon atoms and displaces the electron cloud

**TABLE 1. Materials Properties of Graphene, Si, GaAs, Si, and Hexagonal-BN (h-BN)**

| | thermal conductivity ($W\ m^{-1}\ k^{-1}$) | energy gap $E_g$ (300 K) eV | refractive index $n$ | optical damage threshold (peak intensity of single shot, $MW/cm^2$) | third-order optical nonlinearities (esu) | nonlinear Kerr coefficient ($m^2\ W^{-1}$) |
|---|---|---|---|---|---|---|
| graphene[12,15−17] | 5300 | 0 | 2.6 | $3 \times 10^6$ | $\sim 10^{-7}$ | $10^{-11}$ at 1.55 $\mu$m |
| Si[13] | 149 | 1.11 | 3.44 | 500 | $2.5-5 \times 10^{-11}$ | $(4.5 \pm 1.5) \times 10^{-18}$ at 1.55 $\mu$m |
| GaAs[14,18,19] | 55 | 1.43 | 3.4 | 45 | $\sim 4 \times 10^{-8}$ | $3.3 \times 10^{-17}$ |
| h-BN[20,21] | 20 (∥), 27 (⊥) | 4.0−5.8 | 2.2 | ~500 | $1.36 \times 10^{-14}$ | |

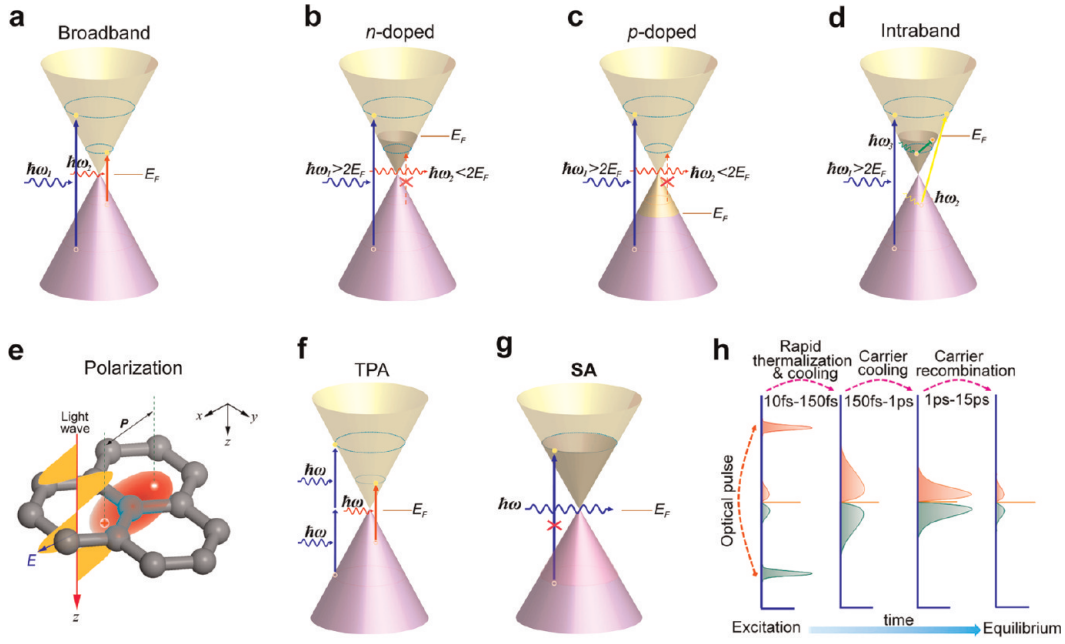


**Figure 1. Schematic diagrams showing possible optical transitions in graphene. (a) In intrinsic graphene, single-photon absorption in terms of symmetric interband transition can take place over a broad wavelength range from visible to infrared. (b) In n-doped graphene, an optical photon ($\hbar\omega_2$) with energy less than $2E_F$ cannot be absorbed because the electron states in resonance in the conduction band are occupied. (c) In p-doped graphene, an optical photon ($\hbar\omega_2$) with energy less than $2E_F$ cannot be absorbed because there are no electrons available for the interband transition. (d) Interband plasmon absorption ($\hbar\omega_2$) and intraband plasmon ($\hbar\omega_3$) absorption with momentum enhancement. (e) Electromagnetic wave ($E$) passing through the graphene lattice and inducing dipole moments ($P$). The displaced electron cloud is shown only for one atom. (f) One-photon and two-photon absorption (TPA) process. (g) Under an intense optical field, the electron states in the conduction band are filled and prevent further optical transition due to Pauli blocking, producing the condition of saturable absorption (SA). (h) Carrier dynamics after photoexcitation showing the processes by which the non-equilibrium electron and hole distributions approach equilibrium. Reproduced from ref 60. Copyright 2008 American Chemical Society.**

with respect to the nucleus, resulting in a net dipole moment (polarization), as shown in Figure 1e. In the simplest case of linear optics regime, the induced displacement ($x$) manifests as electronic polarization ($P$), obeying a linear relationship with the applied field ($E$): $P = \varepsilon_0\chi^{(1)}E$, where $\varepsilon_0$ is the permittivity of free space and $\chi^{(1)}$ is the first-order (linear) susceptibility. In the case of large displacement caused by strong optical field, electronic polarization is significantly nonlinear with respect to displacement as well as applied electric field, which could be described by a Taylor expansion:[44]

$$P = \varepsilon_0(\chi^{(1)}E + \chi^{(2)}E^2 + \chi^{(3)}E^3) + \ldots \quad (6)$$

where $\chi^{(2)}$ and $\chi^{(3)}$ are the second- and third-order nonlinear susceptibilities, associated with nonlinear phenomena such as two-photon absorption (TPA) (Figure 1f), self-focusing, self-phase modulation, saturable absorption (SA) (Figure 1g), optical bistability, *etc.*

Dipole excitations with bound and free electrons induced by a single photon are described by the first-order susceptibility $\chi^{(1)}$, where the real part is correlated to the real part of the refractive index and the imaginary part is related to optical loss or gain. The effective linear susceptibility to optical fields at a frequency $\omega$ can be modulated by applying a dc field across graphene, which changes the refractive index. This linear electro-optic effect is manifested readily in graphene,[32] which forms the basis of a broadband optical modulator recently demonstrated.[26] Due to the inversion symmetry of the graphene unit cell, the second-order susceptibility $\chi^{(2)}$ is generally absent as a result of the cancellation of the

optically excited second-order electrical current at opposite momenta with respect to the Dirac point. However, $\chi^{(2)}$ may be operative in strained,[45] disordered, or functionalized graphene[46−48] in which the bilayer symmetry is broken, thus allowing many possibilities to be exploited in $\chi^{(2)}$ nonlinear electro-optic active material. For example, in graphene derivatives that do not possess inversion symmetry, the application of an optical field at frequency $\omega$ may generate its second harmonic at $2\omega$, which may find important uses for laser frequency doubling as well as high-resolution optical microscopy. More interesting effects may arise by applying the incident field with two frequencies ($\omega_1$ and $\omega_2$), for example, to generate the sum and difference frequencies ($\omega_1 \pm \omega_2$). Recently, Wu *et al.*[49] demonstrated that a giant and tunable second-order nonlinear susceptibility can be observed in bilayer graphene when an in-plane electrical current between source and drain electrodes is introduced to suppress the cancellation of optically induced electric current.

In principle, third-order nonlinear processes are allowed in all materials, whether they process inversion symmetry or not. Most of the optical nonlinearities in graphene are associated with the third-order susceptibility $\chi^{(3)}$. However, $\chi^{(3)}$ is correlated to the polarization per unit volume to the third power of the electric field $E$ and graphene is an infinitesimally thin and isotropic conductivity surface. The classical model fails to fully interpret the optical nonlinearities in graphene, and it is more appropriate to describe the nonlinear response in terms of the $n$th order total integrated sheet current:[15,45,46,50−52]

$$\mathbf{J}_n^{\nu} = \frac{1}{4\pi^2}\int \mathrm{d}\mathbf{p}\mathbf{j}_n^{\nu}N(\varepsilon) \qquad (7)$$

where the thermal factor $N(\varepsilon) = n_F(-\varepsilon) - n_F(\varepsilon) = \tanh(\varepsilon/2k_BT)$, and $\mathbf{j}_n^{\nu} = \psi^{\dagger}\widehat{v}_{\nu}\psi$, where the current operator $\widehat{v}_{\nu} = (\partial H)/(\partial p_{\nu})$ with $\nu = x, y$.

The first-order total current, that is, linear optical response, $\mathbf{J}_1 = e^2E/(4\hbar)$, after converting into real units, coincides with the universal conductance deduced from above-mentioned Kubo formula (eq 2). For a symmetric crystal, $\hat{v}(x) = \hat{v}(-x)$, which implies the second order total sheet current $\mathbf{J}_2 = 0$. The third-order current can be written as[51]

$$\begin{aligned}\mathbf{J}_3 &= \mathbf{J}_3(\omega) + \mathbf{J}_3(3\omega)\\ &= \frac{\sigma_1 e^2 v_F^2 E_0^2}{\hbar^2\omega^4}[N_1(\omega)e^{i\omega t} + N_3(\omega)e^{3i\omega t}] \qquad (8)\end{aligned}$$

where $v_F \approx c/300$, $\sigma_1 = e^2/4\hbar$, the thermal factors $N_1(\omega) = N(\omega)$ and $N_3(\omega) = 13N(\omega/2)/48 - N(\omega)/3 + 45N(3\omega/2)/48$. According to eq 8, the third-order current is a superposition of two third-order terms correlated to three-photon processes, that is, a single frequency term $\mathbf{J}_3(\omega)$ and a third-harmonic generation term $\mathbf{J}_3(3\omega)$. Both of these two terms are inversely proportional to $\omega^4$ and proportional to $E_0^2$ which is the power of the field. They are responsible for a wide variety of optical nonlinear effects in graphene, which includes saturable absorption,[53−56] self-focusing and nonlinear refractive index change (*i.e.*, Kerr effect[16]), optical bistability and switching, and soliton propagation.[57−59]

In practice, the total sheet current in graphene fluctuates with time as well as the pumping conditions (duration of ultrashort intense optical field). The use of ultrashort terahertz laser pulse allows the carrier dynamics in graphene to be investigated,[60] as shown in Figure 1h. The interband optical excitation produces a non-equilibrium carrier population in the valence and conduction bands of graphene. Shortly after photoexcitation (within 10−150 fs), the hot electrons thermalize to form a hot Fermi−Dirac distribution, which will be further cooled by intraband phonon scattering in the following 150 fs to 1 ps. Electron−hole recombination will dominate in the process beyond ~1 ps, which affects the interband conductivity. In view of the nonlinearities in time domain, the interplay between intraband and interband dynamics should be considered to completely describe the nonlinear optical response in graphene.[52]

**Plasmons in Graphene.** Surface plasmons are collective oscillations of electrons at the surface of a conductor, and it can be excited by photon or electron. Noble metals (*e.g.*, Au and Ag) are widely regarded as the best available plasmonic materials, but devices fabricated from these suffer from large Ohmic losses and non-tunability once the geometry of the structure is fixed. Graphene has been recently proposed as a new platform for plasmon waveguiding at infrared frequencies[40−42,61,62] and can be considered as terahertz metamaterials.[63] Photons in the infrared or terahertz domain can be readily coupled to surface plasmons in graphene and form a surface plasmon polariton (SPP) surface wave with many appealing properties,[42,64] such as extreme confinement, tunability *via* electrical gating or chemical doping, and low losses resulting from long lifetime with hundreds of optical cycles. These features make graphene plasmonics an attractive alternative to traditional metal plasmonics. Graphene plasmonics have been demonstrated in photonic metamaterials,[63] light harvesting,[65] optical biosensing,[66] and transformation optics.[67]

The tunability of SPP surface waves in graphene originates from its complex dynamic conductivity determined from the Kubo formula (eq 2), which largely depends on the radian frequency ($\omega$), relaxation time ($\tau_1$) of excited carriers, and chemical potential ($\mu$).[39,68] The imaginary part of dynamic conductivity, which may have a negative or positive signature at different frequency ranges depending on the chemical potential, plays an important role in supporting different types of surface waves. Pristine graphene or graphene with very low chemical potential has a negative $\sigma''$ over a large frequency range, leading to a semiconductor-like behavior, capable of guiding a transverse-electric (TE) electromagnetic SPP surface wave, as illustrated in

Figure 2a.[40,61] At a large chemical potential ($|\mu|>\hbar\omega/2$), it will give a positive $\sigma''$ and graphene will behave like metal thin film capable of supporting a transverse-magnetic (TM) electromagnetic SPP surface wave (Figure 2b), which shows similar behavior to that in noble metals.[47,53−55] Such TM SPP is a type of p-polarized surface plasmon propagating along the sheet with a dispersion relation described by[42]

$$k_{sp} \approx \frac{\hbar^2}{4e^2E_F}(\varepsilon+1)\omega\left(\omega+\frac{i}{\tau_1}\right) \quad (9)$$

The dispersion curves can be obtained by solving the above equation using a semiclassical approach, as shown in Figure 2c, in which the results from random-phase approximation (RPA) are also shown for comparison.[41,69] The quadratic dependence of $k_{sp}$ on $\omega$ is a typical characteristic of 2D electron gases. The field profiles of plasmon in graphene look quite similar to those of surface plasmons in metals except for qualitative differences in electronic dispersions (linear Dirac cones *versus* usual parabolic). The degree of confinement of SPP surface wave in graphene can be written as

$$\lambda_{sp}/\lambda_0 \approx \frac{4\alpha}{\varepsilon+1}\frac{E_F}{\hbar\omega} \quad (10)$$

where $\lambda_0$ is free-space-light wavelength and $\lambda_{sp} = 2\pi/\mathrm{Re}\{k_{sp}\}$ is the wavelength of the SPP surface wave.

Assuming $\lambda_0$ =10 $\mu$m, the chemical potential of graphene $\mu = E_F = 0.15$ eV and $\tau \approx 10^{-13}$ s, thus it gives $\lambda_{sp}$ = 144 nm and the confinement factor (also the effective SPP index, $n_{spp}$) is calculated to be 69.34. The in-plane propagation distance of such TM SPP, given by $1/\mathrm{Im}\{k_{sp}\}$, reaches a value of 2.25 $\mu$m, which is 15.6 times the surface plasmon wavelength.[67] This can be experimentally achieved by fabricating ribbon-like sections of graphene with different chemical potentials, which is analogous to a conventional metal−insulator−metal (MIM) waveguide, as shown in Figure 2d.[67] The chemical potential in a different section of graphene is controlled by different thickness of the dielectric layer. Alternatively, dielectric film with the same thickness but different dielectric constant can be used as a spacer. Clever design in growth and fabrication methods can be applied to tailor the shape of graphene. Some proposed structures of graphene SPP waveguiding structures which mimick the metal/Si waveguides are shown in Figure 2e−g.[64,67]

We should remark that many of the considerations above are still theoretical due to the practical difficulties in exciting and detecting the SPP surface wave in graphene. This is because of the large wave vector mismatch between graphene plasmons and free-space photons. Recently, researchers discovered gate-tunable graphene plasmons by scattering-type scanning near-field optical microscope (s-SNOM) using infrared excitation light (Figure 2h), which provided real-space images of plasmonic field profiles, and they experimentally measured the confinement factor to be 40−60.[70,71] We should take note that these works were carried out on a graphene-oxide-semiconductor (Si) device; the feasibility of optical nanoimaging of graphene plasmons will definitely pave the way for advanced graphene−Si−metal hybrid plasmonic circuits.

**Photonic Applications.** Motivated by the interesting optical properties of graphene, many graphene-based photonic and optoelectronic applications have been developed recently.[9,10] Here we will provide a brief review of the latest development in graphene photonics, which include a graphene waveguide, broadband polarizer,[43] graphene modulator,[26] graphene photodetector,[72−77] surface plasmon enhanced photodetector,[78,79] saturable absorber for mode-locked[80−83] and Q-switched pulse lasers,[84−86] broadband optical limiter,[87] *etc*. We found that most of these photonic devices exhibit broadband performance, which is directly or indirectly correlated with the unique electronic structure in graphene. The broadband operation of these devices ranges from visible to near-infrared (NIR) wavelength and is summarized in Figure 3.

**Broadband Polarizer.** The semimetal nature of graphene inspires researchers to explore its optical waveguide phenomenon. The local dynamic response of ultrathin metal film to electromagnetic wave is described by the Drude model, in which the concentration, effective mass, and scattering rate of electrons are the key parameters. The spectra of electromagnetic modes are sensitive to the electron mass in conventional 2D electrons systems with parabolic dispersion. However, as discussed above, the massless Dirac fermions in graphene modify the plasmon and plasmon polariton spectra and introduce some radically new features.[39,40,61,88] The consequence is that graphene can selectively support either the TM or TE electromagnetic modes depending on its Fermi level and incident energy. This provides the basis for the development of graphene/silica hybrid waveguide, which supports either a TM or TE surface wave selectively, thus transforming unpolarized incident light into polarized light. Such polarization is vital to reducing signal fading and error in coherent optical communications.

In order to fabricate a polarizer which relies on the waveguiding property of graphene, coupling and phase-matching issues have to be considered. Using conventional prism or gratings is possible but lacks high efficiency and is not easy to operate with graphene. Due to the atomic thickness of graphene, it is challenging to realize highly efficient coupling and high-confinement guiding. Recently, researchers successfully coupled wide-band light into graphene film by fabricating a graphene-to-fiber coupler in which graphene grown by chemical vapor deposition

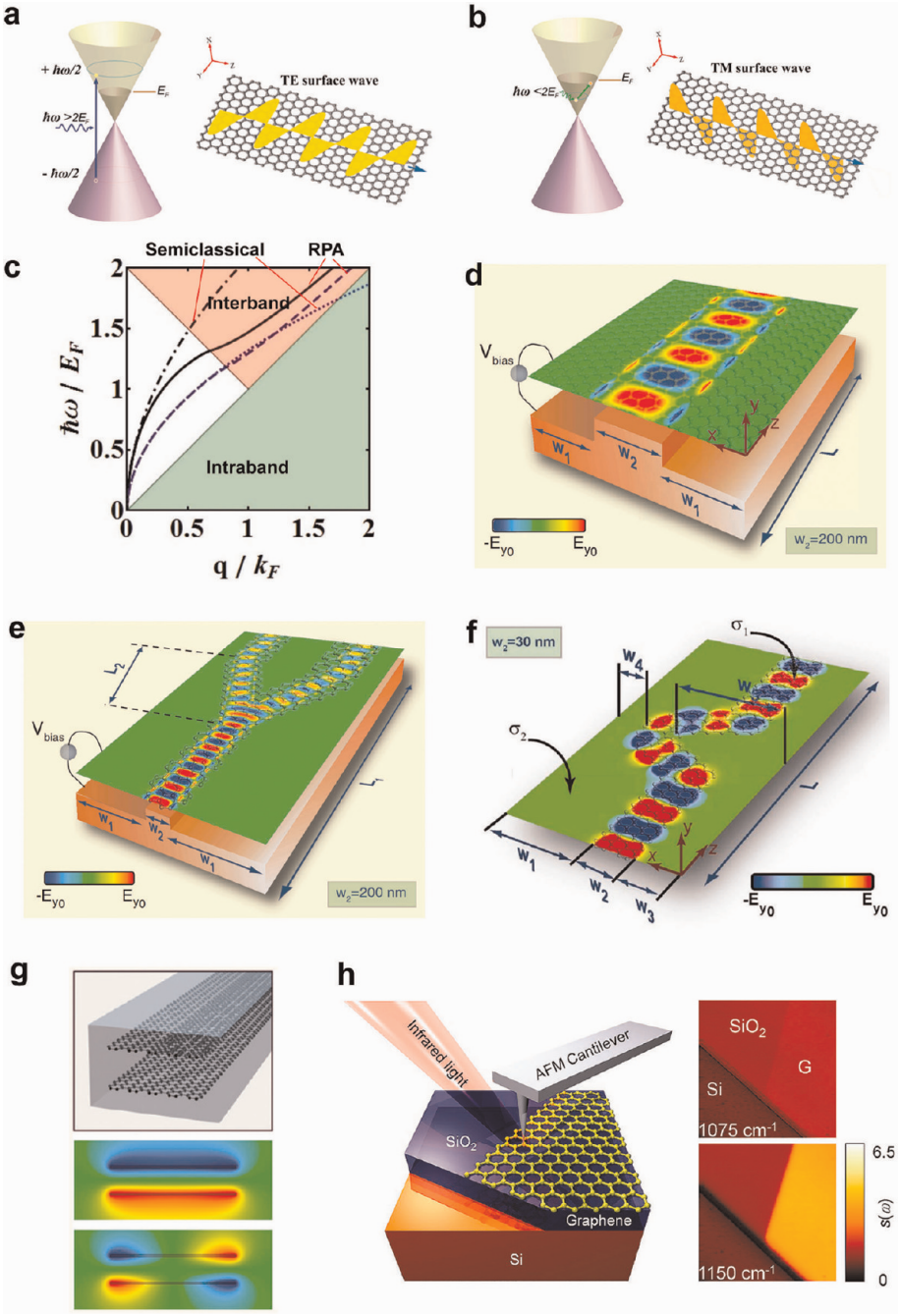


**Figure 2. Graphene plasmons and SPP surface wave. (a) Schematic illustration of interband transition (left) which supports the TE wave propagation (right). (b) Schematic illustration of intraband transition which supports the TM wave propagation (right). (c) Dispersion curves of plasmon in graphene by semiclassic and RPA approaches. For black solid and black dot-dashed lines, graphene is suspended in a vacuum. For blue dashed and blue dotted lines, graphene is on top of dielectric material with $\varepsilon = 4$. Reprinted with permission from ref 41. Copyright 2009 The American Physical Society. (d) Electric field profile ($E_y$) of the TM surface wave at a frequency of 30 THz propagating along the ribbon-like section of graphene with the chemical potential of 0.15 eV ($L$ = 560 nm, $w_1 = w_2$ = 200 nm). (e) Similar to (d), but the TM surface wave is split into two paths along the Y shape graphene junction ($L_1$ = 1077 nm, $L_2$ = 560 nm, $w_1$ =600 nm, $w_2$ = 200 nm). (f) Similar to (d), but the TM surface wave propagates along a bent ribbon-like section of graphene ($L$ = 370 nm, $w_1$ =120 nm, $w_2 = w_4$ = 30 nm, $w_3$ = 60 nm, $w_5$ = 120 nm). Panels d-f reprinted with permission from ref 67. Copyright 2011 The American Association for the Advancement of Science. (g) Schematic illustration of two parallel graphene ribbons embedded in silica (top) with a distance of 5 nm and electric near-field of plasmon modes for two ribbons separated by a distance of 5 nm with energies of 0.15 (middle) and 0.21 eV (bottom). Reproduced from ref 64. Copyright 2012 American Chemical Society. (h) Schematics of s-SNOM on top of graphene/$SiO_2$ interface which is designed to probe Dirac plasmons by IR excitation light. IR near-field nanoscopy images displayed at two different frequencies are shown on the right. Reproduced from ref 71. Copyright 2011 American Chemical Society.**

(CVD) was transferred onto the side-polished optical fiber, as schematically illustrated in Figure 4a.[43] As pristine graphene is used (with slight substrate-induced doping), the TE surface wave is supported whereas the TM

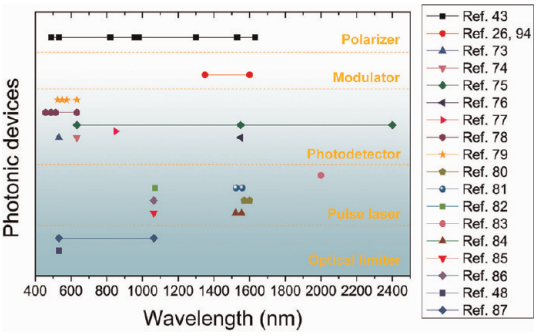


**Figure 3. Broadband operation of graphene-based photonic devices including polarizer, optical modulator, photodetector, pulse laser, and optical limiter.**

wave is scattered *via* leaky modes. The TE-pass polarization effect works over a wide wavelength range from visible to NIR with a large polarization extinction ratio (~27 dB at 1.55 $\mu$m), as shown in Figure 4c. This polarization effect is distinct from that in a metal-clad fiber polarizer with a similar configuration (shown in Figure 4b), in which only the TM wave is supported due to SPP propagation in the metal strip.[89,90]

In principle, the TE-pass polarizer can be switched to TM-pass polarizer once the graphene film is sufficiently doped to shift the chemical potential to a value larger than half excitation energy ($\hbar\omega/2$). For instance, ferroelectric polymers such as polyvinylidene fluoride (PVDF), which has strong dipole moments, can be coated on top of the graphene film and applied as a top gate, as shown in Figure 4d. A small external bias can cause a strong dipole field in PVDF,[91,92] which can further dope graphene and shift the Fermi energy to a level which can support TM SPP at telecommunication wavelength (*e.g.*, 1.55 $\mu$m). Alternatively, a change in the sign of external field can also cause a switchable polarization effect between a TM and TE wave in such an electro-optical device.

**Broadband Optical Modulator.** An optical modulator is a device that is used to vary the fundamental characteristics of a light beam propagating either in free space or in an optical waveguide upon external voltage control. These devices can be amplitude, phase, or polarization modulators. As discussed above, the effective linear susceptibility $\chi^{(1)}$ can be modulated by applying an electric field across graphene, thus causing changes in both the real and imaginary refractive indices. The change in the real part of the refractive index concerns electro-refraction, whereas the change in the imaginary part concerns electro-absorption. The primary effects induced by the electric field include Pockels effect, the Kerr effect, the Franz-Keldysh effect, and the quantum-confined Stark effect (QCSE), and depending on which effect is manifesting, the modulators can be classified as either electro-refractive or electro-absorptive. The unique electronic structure in graphene affords a much stronger electro-absorption effect, which has not yet been observed in bulk materials. When shifting the electronic Fermi level by chemical doping or electric gating, the optical transitions in graphene can be controllably tuned over a wide bandwidth.[32,93]

By integrating graphene with a Si optical waveguide, graphene had been used as the active medium in an optical electro-absorption modulator,[26] as shown in Figure 5a. The coupling strength between the evanescent waves and graphene can be controlled by changing the Fermi level ($E_F$) using an external gate field, which produces changes in the transmission of the optical modulator, as illustrated in Figure 5b.[26] Changing the bias voltage shifts the Fermi level above or below the threshold value ($\hbar\omega/2$), and hence optical interband transitions can be switched "on" or "off". This forms the basis of an electrically controlled optical switch. The optical modulation effect can be observed in optical bandwidth from 1.35 to 1.6 $\mu$m and a very large radio frequency bandwidth up to 1.2 GHz.[26] By constructing an optical modulator with two graphene layers separated by an oxide layer, the modulation depth can be further increased to ~0.16 dB/$\mu$m.[94] The proven modulation efficiency is already comparable to traditional optical modulators made of Si,[95] GeSi,[96] and InGaAs.

Apart from the modulation based on optical interband transition, the modulation of optical intraband transition (or so-called plasmon absorption) is also possible. Andersen *et al.*[97] proposed a TM surface plasmon modulator at long-wavelength IR range ($\lambda$ = 10 $\mu$m), in which an electric back gate is used to change Fermi level in graphene, as shown in Figure 5c. The modulation principle is based on the plasmon losses *versus* carrier density, that is, high or low losses for different carrier densities when the interband absorption of the plasmon energy is allowed or blocked (Figure 5d). The theoretical on/off ratio can reach ~62 dB. In principle, such a modulator should have a much faster switching speed than the modulator based on optical interband transition because the intraband carrier relaxation time ($\tau_1$ < 1 ps) is intrinsically much faster than the interband carrier ($\tau_2$ > 1 ps) relaxation time (see Figure 1h).

The complementary role of graphene to silicon photonics inspires the design of new structures targeted to improve the figures of merit in optical modulation, which include modulation speed and depth (extinction ratio), optical bandwidth, insertion loss, area efficiency (footprint), and power consumption. One demonstration may be a buried-type modulator which consists of dual graphene layers separated by thin BN spacers and sandwiched between single-crystalline Si (bottom) and polycrystalline silicon (top),[24] as shown in Figure 5e. Graphene is placed at the center of the waveguide with maximum light intensity, so as to maximize the modulation depth and lower the power consumption. Another example is a structure with graphene incorporated in the silicon ring resonator

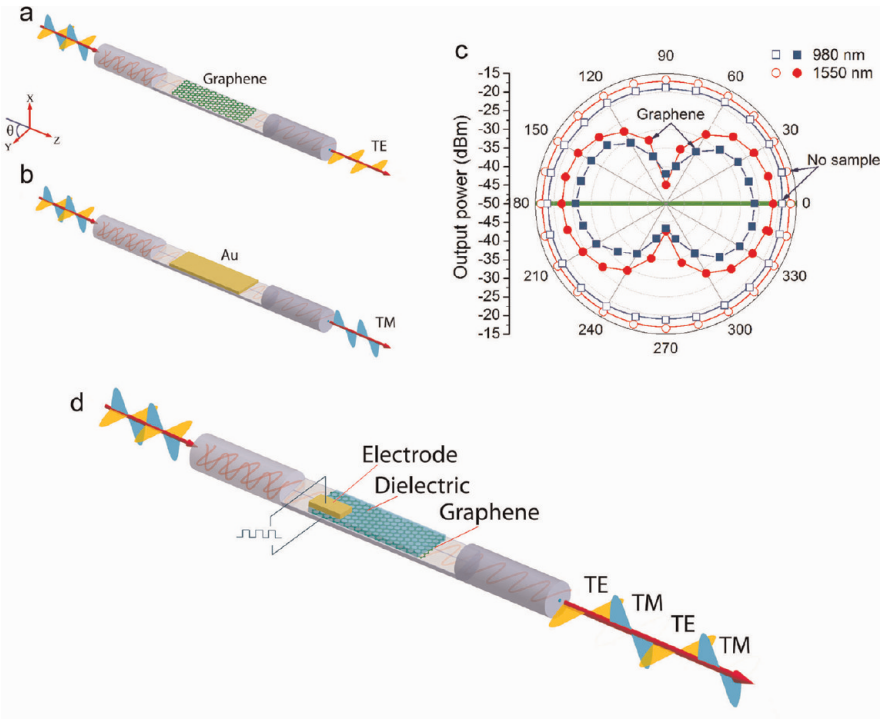


**Figure 4. (a) Schematic illustration of the metal-clad fiber polarizer. (b) Schematic illustration of the graphene-based broad-band polarizer. (c) Polar image measured at 980 and 1550 nm. The green line indicates the project of the graphene film in the *x*−*y* plane (a). Panels a and c reprinted with permission from ref 43. Copyright 2011 Nature Publishing Group. (d) Schematic illustration of a switchable graphene polarizer in which the output polarization state can be controlled by an external electrical field.**

for translating phase variations into intensity variations, as illustrated schematically in Figure 5f. The transmitted signal from the Si/graphene hybrid waveguide can be strongly modulated upon the modification of the resonant wavelength caused by tuning the effective index of the ring waveguide. Graphene can also be coated on a GaAs microdisk resonator to induce whispering gallery mode (Figure 5g), which can be a new type of optomechanical resonators. Lastly, we propose a hybrid graphene/BN quantum confined Stark effect modulator, as shown in Figure 5h. The electrons and holes within the graphene/BN multilayer quantum well locate within a discrete set of energy sub-bands. An external electric field shifts electron and hole states to opposite sides of the energy well, decreases the overlap integral, and thus changes the absorption of the system.

**Broadband Photodetector.** The spectral bandwidth and response time are important figures of merit of a photodetector. The spectral bandwidth is determined by the band gap of the materials, and the response time is correlated to the carrier mobility. Traditional photodetectors based on group IV and III−V semiconductors suffer from limited spectral bandwidth as they are "blind" to photons with energy smaller than the band gap.[98] Graphene can be potentially applied in an ultrafast broadband photodetector because of its exceptionally high carrier mobility and ultra-wideband absorption window.[74−76] The generation and transport of photocarriers in graphene are fundamentally different from that in a semiconductor with a band gap. The absorption of light generates electron−hole pairs in graphene, which has a lifetime of picoseconds before recombination.[53,60] Under an external field, the pairs can be separated and transported to give a detectable photocurrent. Both photovoltaic effect and photothermoelectric effect can contribute to generation of photocurrent in graphene.[9,99,100] The photovoltaic effect relies on the existence of a built-in electric field which helps to accelerate the photogenerated charge carriers toward the electrodes. Such a built-in field can exist when the source and drain contacts on graphene are constructed of metal of different work functions.[25] The photothermoelectric effect is produced by light-induced temperature gradient across an interface between two materials wherein one of the materials has a different Seebeck coefficient.

The IBM group pioneered a graphene-based photodetector with an ultra-broadband photoresponse from 514 to 2400 nm.[72,74−77] They suggested that the operation wavelength range can be further expanded from 300 nm to 6 $\mu$m, which surpasses state-of-the-art photodetectors. Mueller *et al.*[75] demonstrated a graphene photodetector for error-free high-speed optical communications. In their work,[75] interdigitated metal electrodes are deposited on top of graphene to enlarge the light detection region and shorten the transport length of carriers, as shown in Figure 6a. The use of asymmetric metal electrodes with

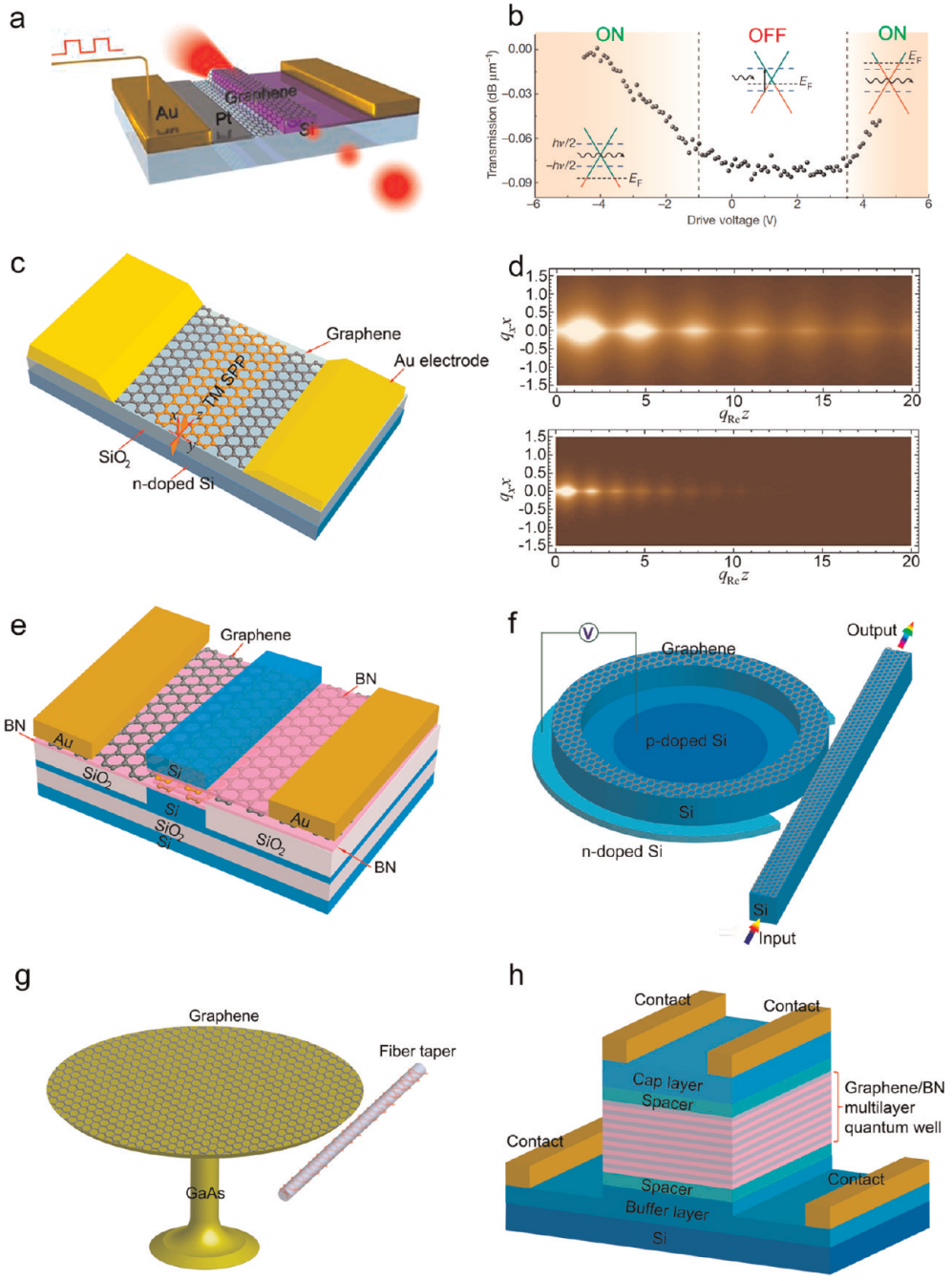


**Figure 5. Graphene-based optical modulator. (a) Graphene-based electro-optical modulator. A monolayer graphene is on top of a silicon bus waveguide, which is separated by a thin $Al_2O_3$ layer. The silicon waveguide is doped and connected to the right Au electrode by a thin layer of silicon. Graphene film is connected to the left Au electrode by a thin layer of Pt. (b) Static electro-optical response of the modulator at different drive voltages. Panels a and b reprinted with permission from ref 43. Copyright 2011 Nature Publishing Group. (c) Schematic structure of graphene plasmon modulator. (d) Propagation of $\lambda_0 = 10\ \mu$m plasmons by RPA approach with different carrier density. Top: Low-loss state with high carrier density. Bottom: High-loss state with low carrier density. Reproduced from ref 97. Copyright 2010 The Optical Society of America. (e) Schematic of a buried-type modulator which consists of dual graphene layers separated by thin BN spacers. (f) Proposed model of graphene-based ring resonator. (g) Graphene-based microdisk resonator. (h) Model of a graphene/boron nitride-based QCSE modulator.**

different doping effects leads to the built-in potential drop within the graphene channel, allowing maximum photocurrent to be detected. The 3 dB frequency bandwidth of 16 GHz was determined from a modulated optical signal at a wavelength of 1550 nm.[75] In principle, a graphene photodetector can potentially operate at speeds over 500 GHz, which is not restricted by the carrier transit time but the RC time constant of the device. From the high photoresponsivity of 6.1 mA $W^{-1}$ and high bandwidth of the photoresponse at tens of gigahertz, it was suggested that photovoltaic effect rather than thermoelectric effect is the dominant

mechanism in their devices because the latter effect is usually limited by the much slower electron cooling process.[25]

The dark current is relatively high in the graphene-only system when it is photoexcited at an external bias, which leads to small photoelectric gain, especially for infrared and terahertz detection under low photon incident energy. In these cases, the presence of a small energy gap can help to suppress the dark current, similar to the case of quantum-well infrared photodetectors. Ryzhii *et al.*[101] proposed a few prototypes based on bilayer graphene in which energy gap can be varied by the transverse electric field (Figure 6b) or graphene nanoribbons in which the energy gap can be tailored by controlling the width of nanoribbons (Figure 6c).[102] One strategy to enhance the responsivity and detectivity is to apply split gates to form the electrically induced p- and n-doped sections within the graphene channel, which operates like the p-i-n junctions in semiconductor photodiodes, as shown in Figure 6d.[103] Another way to suppress the dark current is the incorporation of dielectric materials (such as $TiO_2$[104] and ZnO[105]) on graphene to form a hybrid interface; this can greatly improve the gain due to effective charge injection and separation at the interface.

Another effective approach is to introduce gold–titanium plasmonic nanostructures next to the electrical contacts of a graphene photodetector, as shown in Figure 6e.[78] Due to the built-in potential resulting from different work function of contact metals, the detector is analogous to the traditional p–n junction photodiode. The plasmonic nanostructures are able to convert incident light into plasmonic oscillations and guide electromagnetic energy to the detector. As a result, the efficiency of graphene-based photodetectors can be increased by up to 20 times because of efficient field concentration in the junction area. In another example, Furchi *et al.*[77] recently demonstrated that the responsivity of a graphene photodetector can be increased to a record value of 21 mA/W by monolithically integrating the graphene sheet in a high-finesse Fabry-Pérot microcavity (shown in Figure 6f), in which the optical absorption of graphene is 26-fold enhanced (>60%) due to the resonant interference. Similar concept of using the microcavity to enhance light detection in the graphene transistor has also been proposed by another group.[106] Peres *et al.* have discussed the physics in this field excellently.[107]

It is worth noting that when hot carriers are generated in abundance, the photothermoelectric effect can contribute to the enhancement of the photoresponse. Due to the relatively slow acoustic phonon scattering rate (~10 ns), both theory[108,109] and experiments[100,110] indicate that thermoelectric currents arising from energy transport of hot carriers have a larger contribution than the photovoltaic effect. The photothermoelectric effect can be observed in graphene optoelectronic devices with a dual-gate homojunction[100,111] or a graphene single-bilayer interface junction[112] where there is a difference in thermoelectric power (Seebeck coefficient). For example, in the case of single-bilayer junction, the Dirac point of a single layer is expected to be lower than the bilayer, and the built-in potential difference causes photoexcited electrons to flow from the bilayer to the single layer. However, as the bilayer has larger thermoelectric power originating from its larger density of states, the hot carriers tend to diffuse from single layer to bilayer to maximize the entropy, which leads to current flow of the opposite sign. As a result, the change in sign of the current as a function of gate voltage provides a fingerprint of hot-carrier-dominated transport and carrier multiplication.[109,110] Photoexcitation by ultrafast pulsed laser can identify the contribution of photothermoelectric effect from that of a conventional photovoltaic mechanism.[100] The efficient design of a device which takes advantage of the difference in Seebeck coefficients of materials may lead to enhanced performance in these devices.

**Broadband Saturable Absorber.** The optical loss suffered by a beam of light passing through graphene can be reduced at high optical intensities. This is the property of saturable absorption, which can be used for the generation of short pulses using passive mode locking or Q switching techniques. Even though most semiconductor (*i.e.*, GaAs) or organic materials (*i.e.*, dyes) show saturable absorption, only those which have saturation intensity much lower than the optical damage threshold can be used practically for photonic applications.[113] Semiconductor saturable absorber mirrors (SESAMs) which operate in the reflection mode are widely used as mode lockers. SESAMs are fabricated by integrating the semiconductor coatings into a mirror structure.[114] The main drawbacks of SESAMs are low damage threshold, narrow working wavelength range, and high cost.

Graphene is emerging as a new type of saturable absorber with potential for wide-band operation.[80,81] Interband optical excitation produces a non-equilibrium carrier population in the valence and conduction bands of graphene. When a steady state is reached between population of excited electrons and the electrons relaxing through electron–hole recombination, the absorption will be saturated, as shown in Figure 1g.[115,116] The nonlinear response under interband excitation is affected by several physical processes (shown in Figure 7a[9,117]), which are dependent on the pumping conditions. Under conditions of strong pumping by ultrafast optical pulses, multiple quantum transitions take place and lead to nonlinear regime of energy relaxation and recombination.[56] The direct consequence is a saturation of the transient absorption; that is, the absorption decreases to a steady level with the increase of pumping power. The maximum optical loss is

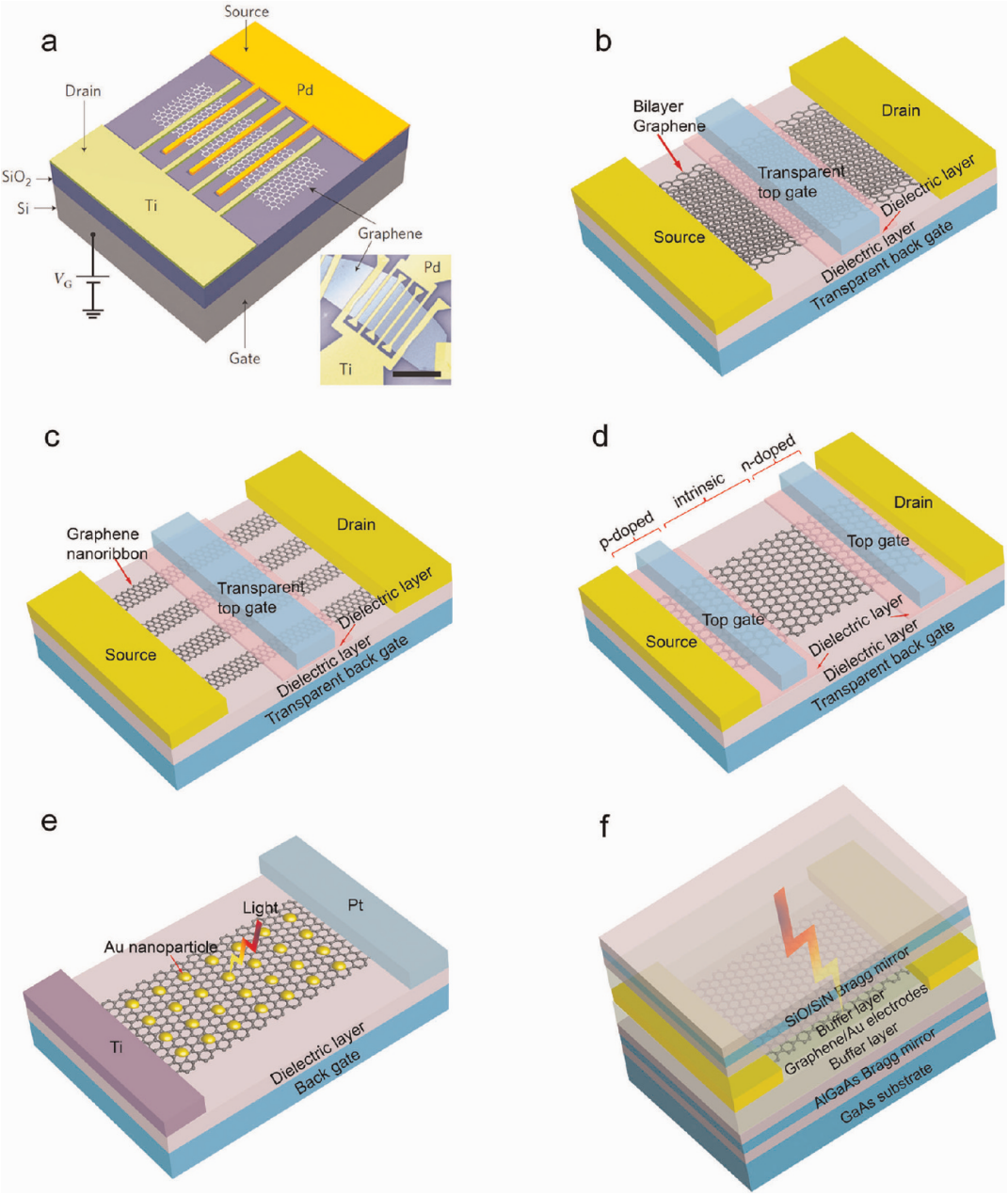


**Figure 6. (a) Schematic illustration of graphene-based photodetector with asymmetric metal contacts. The inset shows the scanning electron microscope image of the photodetector. Reprinted with permission from ref 75. Copyright 2010 Nature Publishing Group. (b) Schematic illustration of graphene bilayer field-effect phototransistor for terahertz and infrared detection. (c) Schematic model of graphene nanoribbon photodetector. (d) Schematic model of photodetector consisting of p-i-n graphene junctions. The p- or n-type doping can be obtained by applying opposite bias at two top gates. (e) Au plasmonic array fabricated on graphene for plasmon resonance enhanced multicolor photodetection. (f) Schematic drawing of graphene microcavity photodetector. Distributed Bragg mirrors are fabricated to form a high-finesse optical cavity which can trap light and enable multiple times passing through the graphene. Adapted from ref 77.**

defined as modulation depth and is associated with third-order optical nonlinearities. The third-order susceptibility $|\chi^3|$ of graphene is measured to be $\sim 10^{-7}$ esu, which is 1 order of magnitude larger than that reported so far for single-walled carbon nanotubes (SWNTs).[15] In principle, monolayer graphene affords the highest saturable absorption for a given amount of material because of the large capacity of Dirac cone to conserve the electrons and holes.[55] Saturable absorbers made of SWNTs[118] or SESAMs,[114] which require either chirality (diameter) control or band gap engineering, are more difficult to fabricate compared to graphene.

The fundamental principle for pulse shaping by graphene is similar to that in semiconductors, as shown schematically in Figure 7b. The broadband nature of graphene in the linear optical regime is also valid at the nonlinear regime. However, unlike the constant linear absorption over a wide spectral range, the saturable

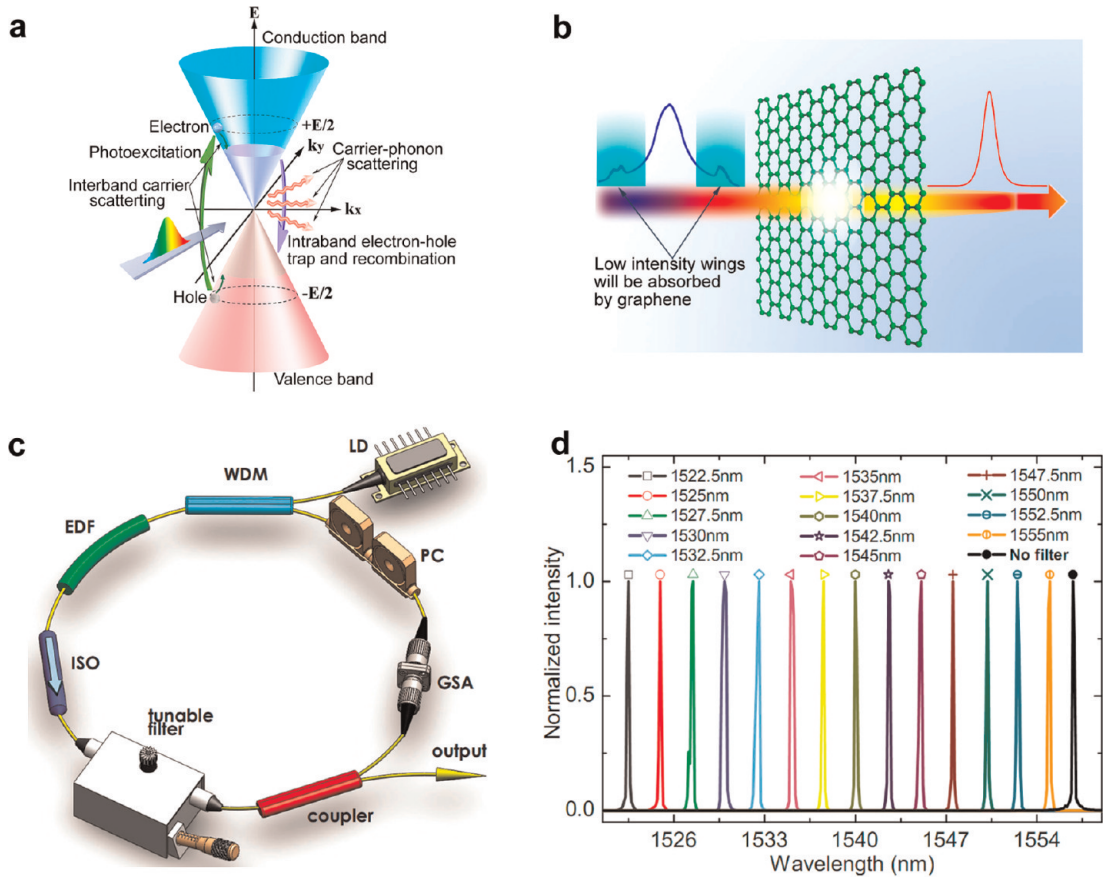


**Figure 7. (a) Schematic illustration of photoexcited electron kinetics in graphene. Reprinted with permission from ref 117. Copyright 2011 American Institute of Physics. (b) Schematic illustration of pulse shaping by graphene saturable absorber. (c) Wide-band-tunable Q-switched laser setup using graphene/PVA composite as saturable absorber. Laser diode (LD), wavelength division multiplexer (WDM), erbium-doped fiber (EDF), isolator (ISO), graphene-based saturable absorber (GSA), and polarization controller (PC). (d) Output spectra at 14 tuning wavelengths from graphene Q-switched fiber laser. Panels c and d reprinted with permission from ref 84. Copyright 2011 American Institute of Physics.**

absorption is wavelength-dependent. A higher pumping power is required to saturate the absorption at higher photon energy (shorter wavelength).[56] This poses considerable challenges for the pulse shaping in the visible range because the saturation intensity is approaching its optical damage threshold. To date, many groups have demonstrated the use of graphene-based saturable absorber in ultrafast pulsed lasers[54,55,85,86,119,120] operating in the telecommunication bands. This is a fast growing area, and the figures of merit for laser performance are continuously being improved. For example, the operation wavelength range has been extended from ~1 $\mu$m,[82] 1.03 $\mu$m,[117] 1.25 $\mu$m,[121] C band (~1530−1565 nm)[80,81,122] to 2 $\mu$m.[83] Sub-200 fs pulse generation[111,112] and high peak power (up to 13.8 kW[117]) laser emission have also been achieved.

Both CVD graphene as well as solution-processed graphene have been used as mode lockers. For the ease of handling a graphene sheet, solution-processed graphene can be combined with polymers to form a physically robust, transparent membrane. This combines the mechanical strength of the polymer-reinforced composite with the optical absorption of organic dyes. Sun *et al.*[81] used a graphene−PVA (polyvinyl alcohol) composite as a saturable absorber for mode-locked laser and achieved 34 nm tunability between 1525 and 1559 nm with the help of a tunable band-pass filter. However, the saturation-induced absorption decrease is very limited (~4.5%), suggesting a small modulation depth. Bao *et al.*[80] fabricated a transparent graphene−organic hybrid membrane that can be handled with a tweezer and fixed on top of an optical fiber. The functionalization of graphene with absorption-enhancing dye molecules maximizes the ratio of saturable-to-nonsaturable absorption, which leads to a large modulation depth of 29%. This modulation depth is close to the saturable absorber made of graphite nanoparticles.[122] The larger modulation depth affords the ease of self-starting the mode-locking above the pump threshold. Therefore, broadband operation with tunable working wavelengths between 1570 and 1600 nm was achieved without using any tunable filter. Mode-locking performance by graphene at ~1 $\mu$m in the fiber laser[82] as well as the solid-state laser[123] further confirmed the broadband nature of graphene-based saturable absorbers. In principle, by saturating the conduction band electrically (*i.e.*,

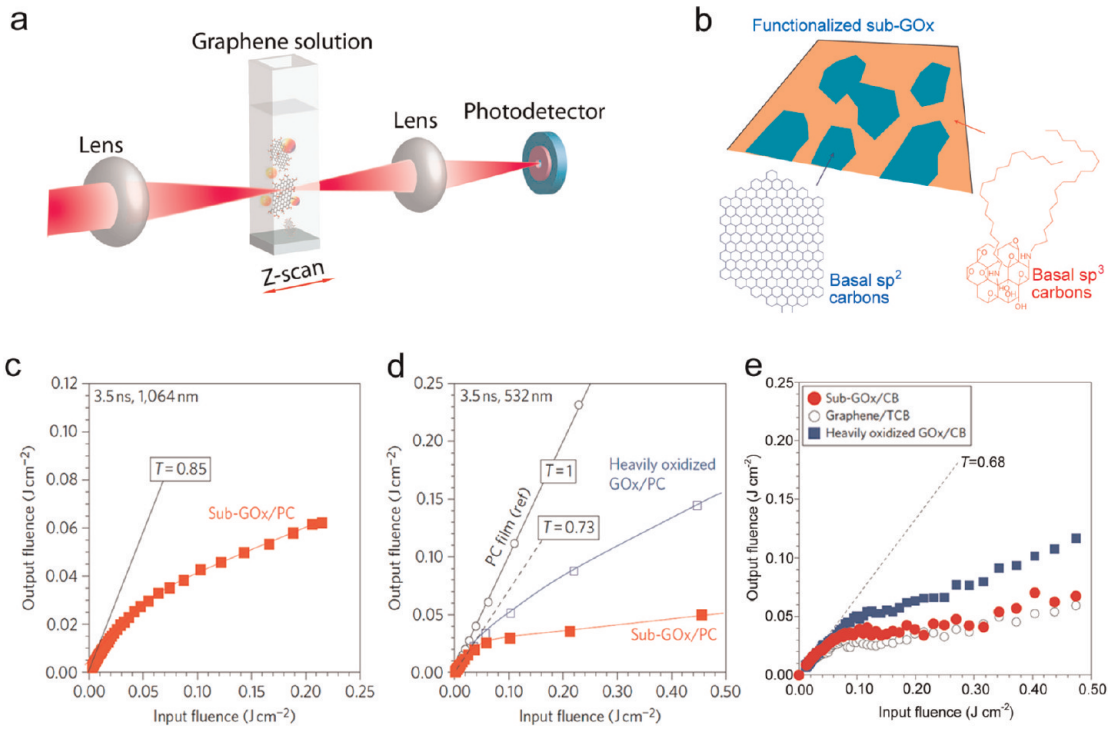


**Figure 8. (a) Schematic illustration of *Z*-scan measurements. (b) Schematic structure of a functionalized sub-$GO_x$ sheet. (c,d) Plot of output *versus* input fluence (red square) for 3.5 ns pulses at 1064 and 532 nm wavelengths, respectively. (e) Nonlinear transmittance characteristics of ultrasonically exfoliated graphene, sub-$GO_x$, and heavily oxidized $GO_x$. Panels b-e reprinted with permission from ref 87. Copyright 2011 Nature Publishing Group.**

shifting the Fermi level), the condition of saturable absorption can be turned off. One interesting possibility is the fabrication of an electro-optic modulator to switch the saturable absorption properties on and off by electrostatic gating; in this case, instabilities in the laser cavity can be quenched in a controllable manner.

Apart from the use of graphene in the mode-locked laser to generate ultrashort laser pulse (picoseconds to femtoseconds), a graphene Q-switched laser is known for generating microsecond to nanosecond pulse with a small width but at high peak power and large pulse energy (tens of nanojoules). Graphene saturable absorber functions as a Q-switcher to modulate the quality factor (Q) of a laser cavity by initiating energy storage, allowing feedback and the process of optical amplification through stimulated emission. Passively Q-switched solid-state lasers with different gain medium (Nd:YAG,[85] Nd:$LuVO_4$,[124] and Nd:$GdVO_4$[86]) have been developed to generate large energy pulses at ~1.06 $\mu$m. Figure 7c shows a representative laser setup used for broadband operation of a graphene Q-switched fiber laser.[84] Using the graphene–PVA composite as an effective saturable absorber, Popa *et al.*[84] demonstrated a wide-band-tunable Q-switched laser from ~1522 to 1555 nm (Figure 7d), which is comparable to the 31 nm range reported for doped crystal Q-switched tunable lasers[125] and much larger than the 5 nm achieved for SWNTs Q-switched lasers.[126] Recently, Cao *et al.* reported a Q-switch fiber laser with an even larger tuning wavelength range up to 50.6 nm.[127] Notably, the graphene Q-switched laser delivers up to ~86.2 nJ energy at ~29 kHz repetition rate. The pulse energy is many times larger than graphene mode-locked fiber lasers[120,128,129] and much larger than values reported for SWNT Q-switched lasers. Such broadband Q-switched lasers are ideal candidates in applications where ultrafast pulses are not necessary, such as material processing, environmental sensing, and biomedical diagnostics.

**Broadband Optical Limiter.** Optical limiters are materials that strongly attenuate intense, potentially dangerous optical beams while exhibiting high transmittance for low-intensity ambient light. Passive optical limiters rely on an effective nonlinear response to dissipate the incident light as a function of its intensity. A good optical limiter should have broadband optical limiting ability, rapid response, and low optical limiting onset threshold. Two main mechanisms are responsible for the optical limiting effect: nonlinear absorption (multiphoton absorption or reverse saturable absorption) and nonlinear scattering (microbubble or microplasma-induced scattering according to Mie scattering theory). Reverse saturable absorption occurs in cases where the excited-stated absorption is stronger than ground-state absorption, and this manifests as an increase in the total absorption at high incident intensity. This is in contrast to the saturable absorption case where the absorption cross section of the ground

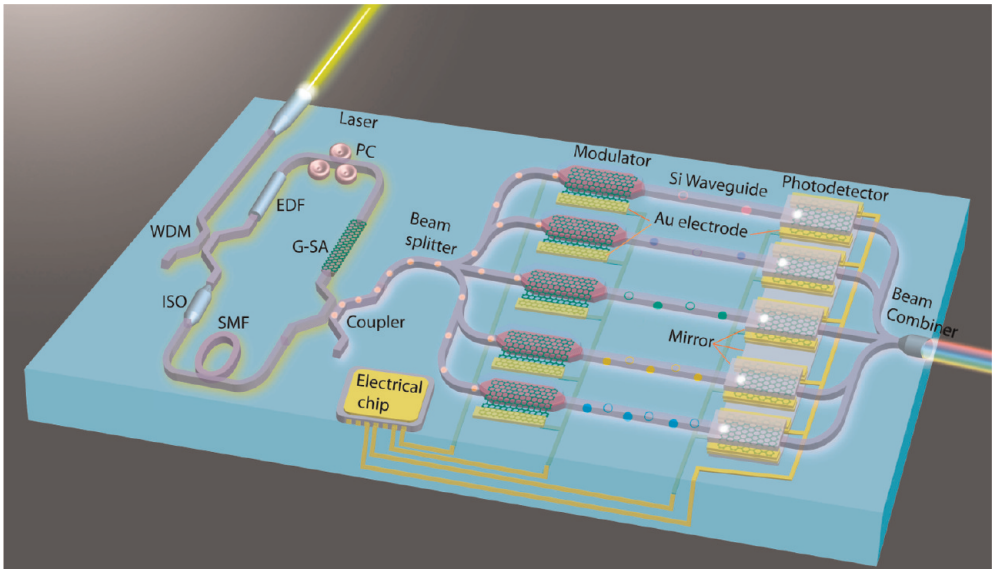


**Figure 9. Schematic illustration of integrated graphene–silicon hybrid photonic circuit, which consists of a graphene mode-locked laser with a ring cavity (left), graphene optical modulator (middle), and microcavity enhanced graphene photodetector (right). In the ring laser, minimized optical components will be used to incorporate into the optical chip, which includes wavelength division multiplexer (WDM), isolator (ISO), single-mode fiber (SMF), erbium-doped fiber (EDF), polarization controller (PC), and graphene-saturable absorber (G-SA). In the optical modulator, graphene is sandwiched between two pieces of the Si waveguide to achieve high modulation depth. Each modulator is separately controlled by the electrical chip so as to encode the optical signals. In the photodetctor, the microcavity with two mirrors is integrated to enhance the light absorption by graphene and the responsivity of the device. The end of the Si waveguide has a wedge shape so as to direct light signals into the photodetector with in-plane configuration. The electrical signals from each photodetector are collected by the electrical chip. The Si waveguide between the modulator and the photodetector can also be prolonged and adapted with optical fiber for long-distance signal transmitting.**

state is stronger compared to the excited state. The lifetimes involved in reverse saturable absorption have to be in the same order as the time between two consecutive pulses to prevent complete relaxation of the excited state to the ground state. In organic molecules, this is aided by slow relaxation and intersystem crossing to the triplet state, such that the next pulse of the pulse train can probe a different population in the electronic states than the first pulse did.[130]

Optical limiting properties of graphene are commonly studied using solution-dispersed graphene oxide derivatives,[48,131,132] where the limiting effects arise from thermally induced nonlinear scattering. These usually involve the formation of scattering centers by microplasmas or microbubbles (Figure 8a), which happen in the nanosecond time scale. Therefore, such a type of thermally induced scattering is operational when the pulse laser operates in the nanosecond time scale. For femtosecond lasers, photoinduced charge transfer between graphene and a dye which occurs at the same time scale may contribute to the optical limiting effect. Due to the ultrafast (femtosecond) relaxation time scale of excited-state electrons in pure graphene, reversed saturable absorption from pristine graphene has not been reported. If the electronic structure of the graphene is modified by chemical functionalization, as in the case of graphene oxide, it may be possible to modify the relaxation dynamics and allow further absorption from the excited state. For example, an alkyl-functionalized substoichiometric graphene oxide was shown to give superior broadband nonlinear optical properties at fluencies well below the damage threshold.[87] Different from pure graphene, the existence of the small $\pi$-conjugated domains surrounded by an insulating matrix affords the confinement of long-lived electron–hole pairs which can interact with surrounding media (shown in Figure 8b), resulting in excited-state absorption (reverse saturable absorption) extending over a wide vis–NIR region. This in turn leads to a new benchmark for optical energy limiting with onset of 10 mJ cm$^{-2}$ for a linear transmittance of 70%, demonstrated in both solvents and polymer composites, as illustrated in Figure 8c–e. As claimed by Lim *et al.*,[87] such sub-stoichiometric graphene oxide (sub-$GO_x$) films exhibit performance which exceeds that of other carbon nanomaterials by a factor of 5–10 times.

The synthesis of a graphene–organic hybrid is motivated by the fact that the formation of new energy dissipation channels *via* photoinduced electron transfer will further expand the optical limiting capability of graphene. The aromatic structure of graphene provides a platform for functionalization with molecular dye with the possibility of forming a charge transfer complex due to donor–acceptor pair interactions. Organic dyes exhibit excellent reverse saturable absorption effects but have relatively low damage threshold and narrow dynamic range,[133] and bonding to

graphene improves the damage threshold due to efficient energy transfer. Nonlinear response can arise from ultrafast photoinduced charge transfer between graphene and the molecular dye, and this is followed by absorption from the charge-separated excited state, thereby leading to an enhanced density of photocarriers and the creation of additional excitation channels with high absorption cross sections.[134]

## CONCLUSIONS AND OUTLOOK

The integration of all-optical and electro-optical devices requires strategies for controlling and manipulating the phase, direction, polarization, and amplitude of optical beams. The ability to control light intensity, as in optical limiting and optical switching, is important in optical communications and optical computing. Methods to control the amplitude and pulse width of light are important in energy modulation. The unique properties of graphene allow it to be used in wide ranging optical control schemes. The fabrication of silicon-based integrated optical circuits, which are designed to assume multiple functions of light creation, routing, modulation, computing, and detection, can be enabled by the broadband optical opacity and tunable dynamical conductivity of graphene. Hopefully, breakthroughs in the direct deposition of graphene on silicon can pave the way for the integration of graphene in hybrid silicon–photonic circuits, as schematically illustrated in Figure 9.

*Conflict of Interest:* The authors declare no competing financial interest.

*Acknowledgment.* The authors thank the NRF-CRP grant "Graphene Related Materials and Devices" R-143-000-360-281. Q.B. acknowledges financial support from the Lee Kuan Yew Postdoctoral Fellowship. We thank N. M. R. Peres for helpful discussion.

## REFERENCES AND NOTES

1. Soref, R. The Past, Present, and Future of Silicon Photonics. *IEEE. J. Sel. Top. Quantum Electron.* **2006**, *12*, 1678–1687.
2. Jalali, B.; Fathpour, S. Silicon Photonics. *J. Lightwave Technol.* **2006**, *24*, 4600–4615.
3. Lipson, M. Guiding, Modulating, and Emitting Light on Silicon - Challenges and Opportunities. *J. Lightwave Technol.* **2005**, *23*, 4222–4238.
4. Jackson, W. B.; Amer, N. M. Direct Measurement of Gap-State Absorption in Hydrogenated Amorphous Silicon by Photothermal Deflection Spectroscopy. *Phys. Rev. B* **1982**, *25*, 5559–5562.
5. Neto, A. H. C.; Guinea, F.; Peres, N. M. R.; Novoselov, K. S.; Geim, A. K. The Electronic Properties of Graphene. *Rev. Mod. Phys.* **2009**, *81*, 109–162.
6. Novoselov, K. S.; Geim, A. K.; Morozov, S. V.; Jiang, D.; Zhang, Y.; Dubonos, S. V.; Grigorieva, I. V.; Firsov, A. A. Electric Field Effect in Atomically Thin Carbon Films. *Science* **2004**, *306*, 666–669.
7. Liao, L.; Lin, Y. C.; Bao, M.; Cheng, R.; Bai, J.; Liu, Y.; Qu, Y.; Wang, K. L.; Huang, Y.; Duan, X. High-Speed Graphene Transistors with a Self-Aligned Nanowire Gate. *Nature* **2010**, *467*, 305–308.
8. Lin, Y. M.; Dimitrakopoulos, C.; Jenkins, K. A.; Farmer, D. B.; Chiu, H. Y.; Grill, A.; Avouris, P. 100-GHz Transistors from Wafer-Scale Epitaxial Graphene. *Science* **2010**, *327*, 662.
9. Bonaccorso, F.; Sun, Z.; Hasan, T.; Ferrari, A. Graphene Photonics and Optoelectronics. *Nat. Photonics* **2010**, *4*, 611–622.
10. Avouris, P. Graphene: Electronic and Photonic Properties and Devices. *Nano Lett.* **2010**, *10*, 4285–4294.
11. Loh, K. P.; Bao, Q.; Eda, G.; Chhowalla, M. Graphene Oxide as a Chemically Tunable Platform for Optical Applications. *Nat. Chem.* **2010**, *2*, 1015–1024.
12. Roberts, A.; Cormode, D.; Reynolds, C.; Newhouse-Illige, T.; Leroy, B. J.; Sandhu, A. S. Response of Graphene to Femtosecond High-Intensity Laser Irradiation. *Appl. Phys. Lett.* **2011**, *99*, 051912.
13. Wang, X.; Shen, Z.; Lu, J.; Ni, X. Laser-Induced Damage Threshold of Silicon in Millisecond, Nanosecond, and Picosecond Regimes. *J. Appl. Phys.* **2010**, *108*, 033103.
14. Garg, A.; Kapoor, A.; Tripathi, K. Laser-Induced Damage Studies in GaAs. *Opt. Laser Technol.* **2003**, *35*, 21–24.
15. Hendry, E.; Hale, P.; Moger, J.; Savchenko, A.; Mikhailov, S. Coherent Nonlinear Optical Response of Graphene. *Phys. Rev. Lett.* **2010**, *105*, 97401.
16. Zhang, H.; Virally, S.; Bao, Q.; Loh, K. P.; Massar, S.; Godbout, N.; Kockaert, P. Large Nonlinear Kerr Effect in Graphene. *Arxiv preprint* **2012**, DOI: arXiv:1203.5527v1.
17. Blake, P.; Hill, E. W.; Neto, A. H. C.; Novoselov, K. S.; Jiang, D.; Yang, R.; Booth, T. J.; Geim, A. K. Making Graphene Visible. *Appl. Phys. Lett.* **2007**, *91*, 063124.
18. Walrod, D.; Auyang, S. Y.; Wolff, P. A.; Sugimoto, M. Observation of Third Order Optical Nonlinearity Due to Intersubband Transitions in AlGaAs/GaAs Superlattices. *Appl. Phys. Lett.* **1991**, *59*, 2932–2934.
19. Said, A.; Sheik-Bahae, M.; Hagan, D. J.; Wei, T.; Wang, J.; Young, J.; Stryland, E. W. V. Determination of Bound-Electronic and Free-Carrier Nonlinearities in ZnSe, GaAs, CdTe, and ZnTe. *J. Opt. Soc. Am. B* **1992**, *9*, 405–414.
20. Cappellini, G.; Satta, G.; Palummo, M.; Onida, G. Optical Properties of BN in Cubic and Layered Hexagonal Phases. *Phys. Rev. B* **2001**, *64*, 035104.
21. Lan, Y. Z.; Cheng, W. D.; Wu, D. S.; Li, X. D.; Zhang, H.; Gong, Y. J.; Shen, J.; Li, F. F. Theoretical Studies of Third-Order Nonlinear Optical Response for $B_{12}N_{12}$, $B_{24}N_{24}$ and $B_{36}N_{36}$ Clusters. *J. Mol. Struct.* **2005**, *730*, 9–15.
22. Rummeli, M. H.; Bachmatiuk, A.; Scott, A.; Borrnert, F.; Warner, J. H.; Hoffman, V.; Lin, J. H.; Cuniberti, G.; Buchner, B. Direct Low-Temperature Nanographene CVD Synthesis over a Dielectric Insulator. *ACS Nano* **2010**, *4*, 4206–4210.
23. Su, C.-Y.; Lu, A.-Y.; Wu, C.-Y.; Li, Y.-T.; Liu, K.-K.; Zhang, W.; Lin, S.-Y.; Juang, Z.-Y.; Zhong, Y.-L.; Chen, F.-R.; *et al.* Direct Formation of Wafer Scale Graphene Thin Layers on Insulating Substrates by Chemical Vapor Deposition. *Nano Lett.* **2011**, *11*, 3612–3616.
24. Kim, K.; Choi, J. Y.; Kim, T.; Cho, S. H.; Chung, H. J. A Role for Graphene in Silicon-Based Semiconductor Devices. *Nature* **2011**, *479*, 338–344.
25. Mueller, T.; Xia, F. N. A.; Avouris, P. Graphene Photodetectors for High-Speed Optical Communications. *Nat. Photonics* **2010**, *4*, 297–301.
26. Liu, M.; Yin, X.; Ulin-Avila, E.; Geng, B.; Zentgraf, T.; Ju, L.; Wang, F.; Zhang, X. A Graphene-Based Broadband Optical Modulator. *Nature* **2011**, *474*, 64–67.
27. Gusynin, V. P.; Sharapov, S. G. Transport of Dirac Quasiparticles in Graphene: Hall and Optical Conductivities. *Phys. Rev. B* **2006**, *73*, 245411.
28. Nair, R. R.; Blake, P.; Grigorenko, A. N.; Novoselov, K. S.; Booth, T. J.; Stauber, T.; Peres, N. M. R.; Geim, A. K. Fine Structure Constant Defines Visual Transparency of Graphene. *Science* **2008**, *320*, 1308–1308.
29. Kuzmenko, A.; Van Heumen, E.; Carbone, F.; Van der Marel, D. Universal Optical Conductance of Graphite. *Phys. Rev. Lett.* **2008**, *100*, 117401.

30. Stauber, T.; Peres, N. M. R.; Geim, A. K. Optical Conductivity of Graphene in the Visible Region of the Spectrum. *Phys. Rev. B* **2008**, *78*, 085432.
31. Nair, R. R.; Blake, P.; Grigorenko, A. N.; Novoselov, K. S.; Booth, T. J.; Stauber, T.; Peres, N. M. R.; Geim, A. K. Fine Structure Constant Defines Visual Transparency of Graphene. *Science* **2008**, *320*, 1308.
32. Wang, F.; Zhang, Y.; Tian, C.; Girit, C.; Zettl, A.; Crommie, M.; Shen, Y. R. Gate-Variable Optical Transitions in Graphene. *Science* **2008**, *320*, 206.
33. De Arco, L. G.; Zhang, Y.; Schlenker, C. W.; Ryu, K.; Thompson, M. E.; Zhou, C. Continuous, Highly Flexible, and Transparent Graphene Films by Chemical Vapor Deposition for Organic Photovoltaics. *ACS Nano* **2010**, *4*, 2865–2873.
34. Wang, Y.; Chen, X.; Zhong, Y.; Zhu, F.; Loh, K. P. Large Area, Continuous, Few-Layered Graphene as Anodes in Organic Photovoltaic Devices. *Appl. Phys. Lett.* **2009**, *95*, 063302.
35. Wang, Y.; Tong, S. W.; Xu, X. F.; Özyilmaz, B.; Loh, K. P. Graphene: Interface Engineering of Layer-by-Layer Stacked Graphene Anodes for High-Performance Organic Solar Cells. *Adv. Mater.* **2011**, *23*, 1475–1475.
36. Hecht, D. S.; Hu, L.; Irvin, G. Emerging Transparent Electrodes Based on Thin Films of Carbon Nanotubes, Graphene, and Metallic Nanostructures. *Adv. Mater.* **2011**, *23*, 1482–1513.
37. Bae, S.; Kim, H.; Lee, Y.; Xu, X.; Park, J. S.; Zheng, Y.; Balakrishnan, J.; Lei, T.; Kim, H. R.; Song, Y. I. Roll-to-Roll Production of 30-Inch Graphene Films for Transparent Electrodes. *Nat. Nanotechnol.* **2010**, *5*, 574–578.
38. Li, Z.; Henriksen, E.; Jiang, Z.; Hao, Z.; Martin, M.; Kim, P.; Stormer, H.; Basov, D. N. Dirac Charge Dynamics in Graphene by Infrared Spectroscopy. *Nat. Phys.* **2008**, *4*, 532–535.
39. Gusynin, V. P.; Sharapov, S. G.; Carbotte, J. P. Unusual Microwave Response of Dirac Quasiparticles in Graphene. *Phys. Rev. Lett.* **2006**, *96*, 256802.
40. Mikhailov, S.; Ziegler, K. New Electromagnetic Mode in Graphene. *Phys. Rev. Lett.* **2007**, *99*, 016803.
41. Jablan, M.; Buljan, H.; Soljačić, M. Plasmonics in Graphene at Infrared Frequencies. *Phys. Rev. B* **2009**, *80*, 245435.
42. Koppens, F. H. L.; Chang, D. E.; García de Abajo, F. J. Graphene Plasmonics: A Platform for Strong Light–Matter Interactions. *Nano Lett.* **2011**, *11*, 3370–3377.
43. Bao, Q.; Zhang, H.; Wang, B.; Ni, Z.; Lim, C. H. Y. X.; Wang, Y.; Tang, D. Y.; Loh, K. P. Broadband Graphene Polarizer. *Nat. Photonics* **2011**, *5*, 411–415.
44. Banerjee, P. P. *Nonlinear Optics: Theory, Numerical Modeling, and Applications*; CRC Press: Boca Raton, FL, 2003.
45. Mishchenko, E. Dynamic Conductivity in Graphene Beyond Linear Response. *Phys. Rev. Lett.* **2009**, *103*, 246802.
46. Mikhailov, S. Non-linear Electromagnetic Response of Graphene. *Europhys. Lett.* **2007**, *79*, 27002.
47. Mikhailov, S.; Ziegler, K. Nonlinear Electromagnetic Response of Graphene: Frequency Multiplication and the Self-Consistent-Field Effects. *J. Phys.: Condens. Matter* **2008**, *20*, 384204.
48. Liu, Z.; Wang, Y.; Zhang, X.; Xu, Y.; Chen, Y.; Tian, J. Nonlinear Optical Properties of Graphene Oxide in Nanosecond and Picosecond Regimes. *Appl. Phys. Lett.* **2009**, *94*, 021902.
49. Wu, S.; Mao, L.; Jones, A. M.; Yao, W.; Zhang, C.; Xu, X. Quantum-Enhanced Tunable Second-Order Optical Nonlinearity in Bilayer Graphene. *Arxiv preprint* **2012**, DOI: arXiv:1201.1952.
50. López-Rodríguez, F.; Naumis, G. Analytic Solution for Electrons and Holes in Graphene under Electromagnetic Waves: Gap Appearance and Nonlinear Effects. *Phys. Rev. B* **2008**, *78*, 201406.
51. Wright, A.; Xu, X.; Cao, J.; Zhang, C. Strong Nonlinear Optical Response of Graphene in the Terahertz Regime. *Appl. Phys. Lett.* **2009**, *95*, 072101.
52. Ishikawa, K. L. Nonlinear Optical Response of Graphene in Time Domain. *Phys. Rev. B* **2010**, *82*, 201402.
53. Bao, Q.; Zhang, H.; Ni, Z.; Wang, Y.; Polavarapu, L.; Shen, Z.; Xu, Q. H.; Tang, D. Y.; Loh, K. P. Monolayer Graphene as a Saturable Absorber in a Mode-Locked Laser. *Nano Res.* **2011**, *4*, 297–307.
54. Bao, Q.; Zhang, H.; Wang, Y.; Ni, Z.; Yan, Y.; Shen, Z. X.; Loh, K. P.; Tang, D. Y. Atomic-Layer Graphene as a Saturable Absorber for Ultrafast Pulsed Lasers. *Adv. Funct. Mater.* **2009**, *19*, 3077–3083.
55. Sun, Z. P.; Hasan, T.; Torrisi, F.; Popa, D.; Privitera, G.; Wang, F. Q.; Bonaccorso, F.; Basko, D. M.; Ferrari, A. C. Graphene Mode-Locked Ultratast Laser. *ACS Nano* **2010**, *4*, 803–810.
56. Vasko, F. T. Saturation of Interband Absorption in Graphene. *Phys. Rev. B* **2010**, *82*, 245422.
57. Belonenko, M.; Lebedev, N.; Tuzalina, O. Y. Electromagnetic Solitons in a System of Graphene Planes with Anderson Impurities. *J. Russ. Laser Res.* **2009**, *30*, 101–108.
58. Dong, H.; Conti, C.; Biancalana, F. Terahertz Relativistic Spatial Solitons in Doped Graphene Metamaterials. *Arxiv preprint* **2011**, DOI: arXiv:1107.5803.
59. Cheh, J.; Zhao, H.; Solitons in Graphene. *Arxiv preprint* **2011**, DOI: arXiv:1107.3696.
60. George, P. A.; Strait, J.; Dawlaty, J.; Shivaraman, S.; Chandrashekhar, M.; Rana, F.; Spencer, M. G. Ultrafast Optical-Pump Terahertz-Probe Spectroscopy of the Carrier Relaxation and Recombination Dynamics in Epitaxial Graphene. *Nano Lett.* **2008**, *8*, 4248–4251.
61. Hanson, G. W. Dyadic Green's Functions and Guided Surface Waves for a Surface Conductivity Model of Graphene. *J. Appl. Phys.* **2008**, *103*, 064302.
62. Nikitin, A. Y.; Guinea, F.; García-Vidal, F.; Martín-Moreno, L. Edge and Waveguide Terahertz Surface Plasmon Modes in Graphene Microribbons. *Phys. Rev. B* **2011**, *84*, 161407.
63. Ju, L.; Geng, B.; Horng, J.; Girit, C.; Martin, M.; Hao, Z.; Bechtel, H. A.; Liang, X.; Zettl, A.; Shen, Y. R.; *et al.* Graphene Plasmonics for Tunable Terahertz Metamaterials. *Nat. Nanotechnol.* **2011**, *6*, 630–634.
64. Christensen, J.; Manjavacas, A.; Thongrattanasiri, S.; Koppens, F. H. L.; García de Abajo, F. J. Graphene Plasmon Waveguiding and Hybridization in Individual and Paired Nanoribbons. *ACS Nano* **2012**, *6*, 431–440.
65. Thongrattanasiri, S.; Koppens, F. H. L.; de Abajo, F. J. G. Total Light Absorption in Graphene. *Arxiv preprint* **2011**, DOI: arXiv:1106.4460.
66. Wu, L.; Chu, H.; Koh, W.; Li, E. Highly Sensitive Graphene Biosensors Based on Surface Plasmon Resonance. *Opt. Express* **2010**, *18*, 14395–14400.
67. Vakil, A.; Engheta, N. Transformation Optics Using Graphene. *Science* **2011**, *332*, 1291–1294.
68. Peres, N. M. R.; Guinea, F.; Castro Neto, A. H. Electronic Properties of Disordered Two-Dimensional Carbon. *Phys. Rev. B* **2006**, *73*, 125411.
69. Hwang, E.; Sarma, S. D. Dielectric Function, Screening, and Plasmons in Two-Dimensional Graphene. *Phys. Rev. B* **2007**, *75*, 205418.
70. Fei, Z.; Rodin, A. S.; Andreev, G. O.; Bao, W.; McLeod, A. S.; Wagner, M.; Zhang, L. M.; Zhao, Z.; Dominguez, G.; Thiemens, M.; *et al.* Gate-Tuning of Graphene Plasmons Revealed by Infrared Nano-Imaging. *Arxiv preprint* **2012**, DOI: arXiv:1202.4993.
71. Fei, Z.; Andreev, G. O.; Bao, W.; Zhang, L. M.; McLeod, A. S.; Wang, C.; Stewart, M. K.; Zhao, Z.; Dominguez, G.; Thiemens, M.; *et al.* Infrared Nanoscopy of Dirac Plasmons at the Graphene–$SiO_2$ Interface. *Nano Lett.* **2011**, *11*, 4701–4705.
72. Mueller, T.; Xia, F.; Freitag, M.; Tsang, J.; Avouris, P. Role of Contacts in Graphene Transistors: A Scanning Photocurrent Study. *Phys. Rev. B* **2009**, *79*, 245430.
73. Park, J.; Ahn, Y.; Ruiz-Vargas, C. Imaging of Photocurrent Generation and Collection in Single-Layer Graphene. *Nano Lett.* **2009**, *9*, 1742–1746.
74. Xia, F.; Mueller, T.; Golizadeh-Mojarad, R.; Freitag, M.; Lin, Y.; Tsang, J.; Perebeinos, V.; Avouris, P. Photocurrent Imaging and Efficient Photon Detection in a Graphene Transistor. *Nano Lett.* **2009**, *9*, 1039–1044.

75. Mueller, T.; Xia, F.; Avouris, P. Graphene Photodetectors for High-Speed Optical Communications. *Nat. Photonics* **2010**, *4*, 297–301.
76. Xia, F.; Mueller, T.; Lin, Y.; Valdes-Garcia, A.; Avouris, P. Ultrafast Graphene Photodetector. *Nat. Nanotechnol.* **2009**, *4*, 839–843.
77. Furchi, M.; Urich, A.; Pospischil, A.; Lilley, G.; Unterrainer, K.; Detz, H.; Klang, P.; Andrews, A. M.; Schrenk, W.; Strasser, G. *et al.* Microcavity-Integrated Graphene Photodetector. *Arxiv preprint* **2011**, DOI: arXiv:1112.1549.
78. Echtermeyer, T. J.; Britnell, L.; Jasnos, P. K.; Lombardo, A.; Gorbachev, R. V.; Grigorenko, A. N.; Geim, A. K.; Ferrari, A. C.; Novoselov, K. S. Strong Plasmonic Enhancement of Photovoltage in Graphene. *Nat. Commun.* **2011**, *2*, 458.
79. Liu, Y.; Cheng, R.; Liao, L.; Zhou, H.; Bai, J.; Liu, G.; Liu, L.; Huang, Y.; Duan, X. Plasmon Resonance Enhanced Multicolour Photodetection by Graphene. *Nat. Commun.* **2011**, *2*, 579.
80. Bao, Q.; Zhang, H.; Yang, J. X.; Wang, S.; Tang, D. Y.; Jose, R.; Ramakrishna, S.; Lim, C. T.; Loh, K. P. Graphene–Polymer Nanofiber Membrane for Ultrafast Photonics. *Adv. Funct. Mater.* **2010**, *20*, 782–791.
81. Sun, Z. P.; Popa, D.; Hasan, T.; Torrisi, F.; Wang, F. Q.; Kelleher, E. J. R.; Travers, J. C.; Nicolosi, V.; Ferrari, A. C. A Stable, Wideband Tunable, near Transform-Limited, Graphene-Mode-Locked, Ultrafast Laser. *Nano Res.* **2010**, *3*, 653–660.
82. Zhao, L.; Tang, D. Y.; Zhang, H.; Wu, X.; Bao, Q.; Loh, K. P. Dissipative Soliton Operation of an Ytterbium-Doped Fiber Laser Mode Locked with Atomic Multilayer Graphene. *Opt. Lett.* **2010**, *35*, 3622–3624.
83. Liu, J.; Wang, Y. G.; Qu, Z. S.; Zheng, L. H.; Su, L. B.; Xu, J. Graphene Oxide Absorber for 2 $\mu$m Passive Mode-Locking Tm:$YAlO_3$ Laser. *Laser Phys. Lett.* **2012**, *9*, 15–19.
84. Popa, D.; Sun, Z.; Hasan, T.; Torrisi, F.; Wang, F.; Ferrari, A. Graphene Q-Switched, Tunable Fiber Laser. *Appl. Phys. Lett.* **2011**, *98*, 073106.
85. Yu, H. H.; Chen, X. F.; Zhang, H. J.; Xu, X. G.; Hu, X. B.; Wang, Z. P.; Wang, J. Y.; Zhuang, S. D.; Jiang, M. H. Large Energy Pulse Generation Modulated by Graphene Epitaxially Grown on Silicon Carbide. *ACS Nano* **2010**, *4*, 7582–7586.
86. Li, X. L.; Xu, J. L.; Wu, Y. Z.; He, J. L.; Hao, X. P. Large Energy Laser Pulses with High Repetition Rate by Graphene Q-Switched Solid-State Laser. *Opt. Express* **2011**, *19*, 9950–9955.
87. Lim, G.-K.; Chen, Z.-L.; Clark, J.; Goh, R. G. S.; Ng, W.-H.; Tan, H.-W.; Friend, R. H.; Ho, P. K. H.; Chua, L.-L. Giant Broadband Nonlinear Optical Absorption Response in Dispersed Graphene Single Sheets. *Nat. Photonics* **2011**, *5*, 554–560.
88. Ryzhii, V.; Satou, A.; Otsuji, T. Plasma Waves in Two-Dimensional Electron–Hole System in Gated Graphene Heterostructures. *J. Appl. Phys.* **2007**, *101*, 024509.
89. Feth, J.; Chang, C. Metal-Clad Fiber-Optic Cutoff Polarizer. *Opt. Lett.* **1986**, *11*, 386–388.
90. Dyott, R. B.; Bello, J.; Handerek, V. A. Indium-Coated D-Shaped-Fiber Polarizer. *Opt. Lett.* **1987**, *12*, 287–289.
91. Lee, Y.-L.; Kim, S.; Park, C.; Ihm, J.; Son, Y.-W. Controlling Half-Metallicity of Graphene Nanoribbons by Using a Ferroelectric Polymer. *ACS Nano* **2010**, *4*, 1345–1350.
92. Zheng, Y.; Ni, G. X.; Bae, S.; Cong, C. X.; Kahya, O.; Toh, C. T.; Kim, H. R.; Im, D.; Yu, T.; Ahn, J. H. Wafer-Scale Graphene/Ferroelectric Hybrid Devices for Low-Voltage Electronics. *Europhys. Lett.* **2011**, *93*, 17002.
93. Li, Z.; Henriksen, E.; Jiang, Z.; Hao, Z.; Martin, M.; Kim, P.; Stormer, H.; Basov, D. Dirac Charge Dynamics in Graphene by Infrared Spectroscopy. *Nat. Phys.* **2008**, *4*, 532–535.
94. Liu, M.; Yin, X.; Zhang, X. Double-Layer Graphene Optical Modulator. *Nano Lett.* **2012**, *12*, 1482–1485.
95. Reed, G.; Mashanovich, G.; Gardes, F.; Thomson, D. Silicon Optical Modulators. *Nat. Photonics* **2010**, *4*, 518–526.
96. Liu, J.; Beals, M.; Pomerene, A.; Bernardis, S.; Sun, R.; Cheng, J.; Kimerling, L. C.; Michel, J. Waveguide-Integrated, Ultralow-Energy Gesi Electro-absorption Modulators. *Nat. Photonics* **2008**, *2*, 433–437.
97. Andersen, D. R. Graphene-Based Long-Wave Infrared Tm Surface Plasmon Modulator. *J. Opt. Soc. Am. B* **2010**, *27*, 818–823.
98. Saleh, B. E. A.; Teich, M. C. *Fundamentals of Photonics*; John Wiley & Sons: New York, 2007.
99. Basko, D. A Photothermoelectric Effect in Graphene. *Science* **2011**, *334*, 610–611.
100. Sun, D.; Aivazian, G.; Jones, A. M.; Ross, J. S.; Yao, W.; Cobden, D.; Xu, X. Ultrafast Hot-Carrier-Dominated Photocurrent in Graphene. *Nat. Nanotechnol.* **2012**, *7*, 114–118.
101. Ryzhii, V.; Ryzhii, M. Graphene Bilayer Field-Effect Phototransistor for Terahertz and Infrared Detection. *Phys. Rev. B* **2009**, *79*, 245311.
102. Ryzhii, V.; Ryzhii, M.; Ryabova, N.; Mitin, V.; Otsuji, T. Graphene Nanoribbon Phototransistor: Proposal and Analysis. *Jpn. J. Appl. Phys.* **2009**, *48*, 04C144.
103. Ryzhii, V.; Ryzhii, M.; Mitin, V.; Otsuji, T. Terahertz and Infrared Photodetection Using Pin Multiple-Graphene-Layer Structures. *J. Appl. Phys.* **2010**, *107*, 054512.
104. Manga, K. K.; Wang, S.; Jaiswal, M.; Bao, Q.; Loh, K. P. High-Gain Graphene-Titanium Oxide Photoconductor Made from Inkjet Printable Ionic Solution. *Adv. Mater.* **2010**, *22*, 5265–5270.
105. Yang, H. Y.; Son, D. I.; Kim, T. W.; Lee, J. M.; Park, W. I. Enhancement of the Photocurrent in Ultraviolet Photodetectors Fabricated Utilizing Hybrid Polymer–ZnO Quantum Dot Nanocomposites Due to an Embedded Graphene Layer. *Org. Electron.* **2010**, *11*, 1313–1317.
106. Engel, M.; Steiner, M.; Lombardo, A.; Ferrari, A. C.; Loehneysen, H.; Avouris, P.; Krupke, R. Light–Matter Interaction in a Microcavity-Controlled Graphene Transistor. *Arxiv preprint* **2011**, DOI: arXiv:1112.1380.
107. Peres, N. M. R.; Ferreira, A.; Ribeiro, R. M.; Stauber, T. An Efficient Graphene-Based Photodetector with Two Cavities. *Arxiv preprint* **2012**, DOI: arXiv:1201.3175.
108. Kim, R.; Perebeinos, V.; Avouris, P. Relaxation of Optically Excited Carriers in Graphene. *Phys. Rev. B* **2011**, *84*, 075449.
109. Song, J. C. W.; Rudner, M. S.; Marcus, C. M.; Levitov, L. Hot Carrier Transport and Photocurrent Response in Graphene. *Nano Lett.* **2011**, *11*, 4688–4692.
110. Gabor, N. M.; Song, J. C. W.; Ma, Q.; Nair, N. L.; Taychatanapat, T.; Watanabe, K.; Taniguchi, T.; Levitov, L. S.; Jarillo-Herrero, P. Hot Carrier-Assisted Intrinsic Photoresponse in Graphene. *Science* **2011**, *334*, 648–652.
111. Lemme, M. C.; Koppens, F. H. L.; Falk, A. L.; Rudner, M. S.; Park, H.; Levitov, L. S.; Marcus, C. M. Gate-Activated Photoresponse in a Graphene p–n Junction. *Nano Lett.* **2011**, *11*, 4134–4137.
112. Xu, X.; Gabor, N. M.; Alden, J. S.; van der Zande, A. M.; McEuen, P. L. Photo-thermoelectric Effect at a Graphene Interface Junction. *Nano Lett.* **2009**, *10*, 562–566.
113. Keller, U. Recent Developments in Compact Ultrafast Lasers. *Nature* **2003**, *424*, 831–838.
114. Keller, U.; Weingarten, K. J.; Kartner, F. X.; Kopf, D.; Braun, B.; Jung, I. D.; Fluck, R.; Honninger, C.; Matuschek, N.; derAu, J. A. Semiconductor Saturable Absorber Mirrors (SESAM's) for Femtosecond to Nanosecond Pulse Generation in Solid-State Lasers. *IEEE J. Sel. Top. Quantum Electron.* **1996**, *2*, 435–453.
115. Vasko, F. T.; Ryzhii, V. Photoconductivity of Intrinsic Graphene. *Phys. Rev. B* **2008**, *77*, 195433.
116. Satou, A.; Vasko, F. T.; Ryzhii, V. Nonequilibrium Carriers in Intrinsic Graphene under Interband Photoexcitation. *Phys. Rev. B* **2008**, *78*, 115431.
117. Xu, J.-L.; Li, X.-L.; He, J.-L.; Hao, X.-P.; Wu, Y.-Z.; Yang, Y.; Yang, K.-J. Performance of Large-Area Few-Layer Graphene Saturable Absorber in Femtosecond Bulk Laser. *Appl. Phys. Lett.* **2011**, *99*, 261107.
118. Hasan, T.; Sun, Z.; Wang, F.; Bonaccorso, F.; Tan, P. H.; Rozhin, A. G.; Ferrari, A. C. Nanotube–Polymer Composites for Ultrafast Photonics. *Adv. Mater.* **2009**, *21*, 3874–3899.
119. Zhang, H.; Bao, Q.; Tang, D.; Zhao, L.; Loh, K. P. Large Energy Soliton Erbium-Doped Fiber Laser with a Graphene–Polymer Composite Mode Locker. *Appl. Phys. Lett.* **2009**, *95*, 141103.

120. Song, Y.-W.; Jang, S.-Y.; Han, W.-S.; Bae, M.-K. Graphene Mode-Lockers for Fiber Lasers Functioned with Evanescent Field Interaction. *Appl. Phys. Lett.* **2010**, *96*, 051122.
121. Cho, W. B.; Kim, J. W.; Lee, H. W.; Bae, S.; Hong, B. H.; Choi, S. Y.; Baek, I. H.; Kim, K.; Yeom, D.-I.; Rotermund, F. High-Quality, Large-Area Monolayer Graphene for Efficient Bulk Laser Mode-Locking near 1.25 $\mu$m. *Opt. Lett.* **2011**, *36*, 4089–4091.
122. Lin, G. R.; Lin, Y. C. Directly Exfoliated and Imprinted Graphite Nano-particle Saturable Absorber for Passive Mode-Locking Erbium-Doped Fiber Laser. *Laser Phys. Lett* **2011**, *8*, 880–886.
123. Tan, W.; Su, C.; Knize, R.; Xie, G.; Li, L.; Tang, D. Mode Locking of Ceramic Nd:Yttrium Aluminum Garnet with Graphene as a Saturable Absorber. *Appl. Phys. Lett.* **2010**, *96*, 031106.
124. Yu, H.; Chen, X.; Hu, X.; Zhuang, S.; Wang, Z.; Xu, X.; Wang, J.; Zhang, H.; Jiang, M. Graphene as a Q-Switcher for Neodymium-Doped Lutetium Vanadate Laser. *Appl. Phys. Exp.* **2011**, *4*, 022704.
125. Laroche, M.; Chardon, A. M.; Nilsson, J.; Shepherd, D. P.; Clarkson, W. A.; Girard, S.; Moncorgé, R. Compact Diode-Pumped Passively Q-Switched Tunable Er-Yb Double-Clad Fiber Laser. *Opt. Lett.* **2002**, *27*, 1980–1982.
126. Zhou, D. P.; Wei, L.; Dong, B.; Liu, W. K. Tunable Passively Q-Switched Erbium-Doped Fiber Laser with Carbon Nanotubes as a Saturable Absorber. *IEEE Photonics Technol. Lett.* **2010**, *22*, 9–11.
127. Cao, W. J.; Wang, H. Y.; Luo, A. P.; Luo, Z. C.; Xu, W. C. Graphene-Based, 50 nm Wide-Band Tunable Passively Q-Switched Fiber Laser. *Laser Phys. Lett.* **2012**, *9*, 54–58.
128. Sun, Z.; Hasan, T.; Torrisi, F.; Popa, D.; Privitera, G.; Wang, F.; Bonaccorso, F.; Basko, D. M.; Ferrari, A. C. Graphene Mode-Locked Ultrafast Laser. *ACS Nano* **2010**, *4*, 803–810.
129. Zhang, H.; Tang, D. Y.; Zhao, L. M.; Bao, Q. L.; Loh, K. P. Large Energy Mode Locking of an Erbium-Doped Fiber Laser with Atomic Layer Graphene. *Opt. Express* **2009**, *17*, 17630–17635.
130. Tutt, L. W.; Boggess, T. F. A Review of Optical Limiting Mechanisms and Devices Using Organics, Fullerenes, Semiconductors and Other Materials. *Prog. Quantum Electron.* **1993**, *17*, 299–338.
131. Zhou, Y.; Bao, Q. L.; Tang, L. A. L.; Zhong, Y. L.; Loh, K. P. Hydrothermal Dehydration for the Green Reduction of Exfoliated Graphene Oxide to Graphene and Demonstration of Tunable Optical Limiting Properties. *Chem. Mater.* **2009**, *21*, 2950–2956.
132. Feng, M.; Zhan, H.; Chen, Y. Nonlinear Optical and Optical Limiting Properties of Graphene Families. *Appl. Phys. Lett.* **2010**, *96*, 033107.
133. O'Flaherty, S. M.; Hold, S. V.; Cook, M. J.; Torres, T.; Chen, Y.; Hanack, M.; Blau, W. J. Molecular Engineering of Peripherally and Axially Modified Phthalocyanines for Optical Limiting and Nonlinear Optics. *Adv. Mater.* **2003**, *15*, 19–32.
134. Balapanuru, J.; Yang, J. X.; Xiao, S.; Bao, Q. L.; Jahan, M.; Polavarapu, L.; Wei, J.; Xu, Q. H.; Loh, K. P. A Graphene Oxide−Organic Dye Ionic Complex with DNA-Sensing and Optical-Limiting Properties. *Angew. Chem., Int. Ed.* **2010**, *49*, 6549–6553.